Investigation of Solar Cells Performance by AMPS-1D Simulation

by

Md. Nawshad Siddique
(112467)
Al Shahriar Shaien
(112471)
Shaon Rahman
(112469)
Md. Musfiqur Rahman
(112468)

BACHELOR OF

SCIENCE IN

ELECTRICAL AND ELECTRONIC ENGINEERING

Department of Electrical and Electronic Engineering
Islamic University of Technology (IUT)
Board Bazar, Gazipur-1704, Bangladesh.

August, 2015.

CERTIFICATE OF APPROVAL

The thesis titled '**Investigation of Solar Cells Performance by AMPS-1D Simulation'** submitted by Md. Nawshad Siddique (112467), Al Shahriar Shaien (112471), Shaon Rahman (112469), Md Musfiqur Rahman (112468) of academic year 2014-15 has been found as satisfactory and accepted as partial fulfillment of the requirement for the Degree of BACHELOR OF SCIENCE IN ELECTRICAL AND ELECTRONIC ENGINEERING.

Board of Examiners:

_____

Dr. Md. Ashraful Hoque — Supervisor
Professor
Electrical and Electronic Engineering Department
Islamic University of Technology (IUT), Gazipur.

_____

Mohammad Tanvirul Ferdaous — Co-Supervisor
Lecturer,
Electrical and Electronic Engineering Department
Islamic University of Technology (IUT), Gazipur.

Declaration of Candidate

It is hereby declared that this thesis report or any part of it has not been submitted elsewhere for the award of any Degree or Diploma.

_____

Dr. Md. Ashraful Hoque
Professor
Electrical and Electronic Engineering Department
Islamic University of Technology (IUT)
Date:

_____

Al Shahriar Shaien
Student No.: 112471
Academic Year: 2014-2015

_____

Nawshad Siddique
Student No.: 112467
Academic Year: 2014-2015

_____

Md Musfiqur Rahman
Student No : 112468
Academic Year: 2014-2015

_____

Shaon Rahman
Student No : 112469
Academic Year: 2014-2015

Dedicated to my parents.

Table of Contents

List of Figures

List of Tables

Symbols & Abbreviations

I	Current (A)
I_L	Photocurrent (A)
I_F	Forward current (A)
I_S	Saturation current (A)
n	Ideality factor
k	Boltzmann constant (JK^{-1})
T	Absolute temperature (K)
q	Charge of an electron (C)
I_{sc}	Short-circuit current (A)
V_{oc}	Open-circuit voltage (V)
P_m	Maximum output power (W)
V_m	Voltage at maximum power point (V)
I_m	Current at maximum power point (A)
FF	Fill Factor
V_{ocn}	Normalized open-circuit voltage (V)
η	Energy conversion efficiency (%)
E	Solar irradiance (W/cm^2)
A	Area of the solar cell (cm^2)
J_{sc}	Short-circuit current density (A/cm^2)

Acknowledgements

I am grateful to my thesis supervisor, Dr. Md. Fokhrul Islam, for his continuous guidance and motivation in completing my thesis. His constant demand for making the work more and more elaborate finally resulted in satisfactory outcomes. I extend my gratitude to all faculty members of EEE department of IUT, OIC for being sources of inspiration and guidance. I would like to thank Professor Dr. Nowshad Amin of the National University of Malaysia (UKM) for providing necessary information and guidance about CdTe solar cells and a helpful introduction to AMPS 1D.

Abstract

Energy conversion efficiency is a major issue for photovoltaic cells today. Researchers are continuously trying to improve the efficiency level of photovoltaic devices by introducing new materials and advanced concepts. The target is to reach a high efficiency level within affordable cost, which will lead to a mass generation of electricity using photovoltaic devices.

In this work, a new structure of CdS/CdTe based solar cell is proposed, where two of the fundamental drawbacks of traditional CdS/CdTe cell are addressed. The relatively low bandgap of CdS window layer, along with a significant lattice mismatch between CdS and CdTe decrease the efficiency of conventional CdS/CdTe solar cell. This work proposes a novel structure where both window (CdS) and absorber (CdTe) layer are replaced by two II-VI ternary alloys, namely, $Cd_{1-x}Zn_xS$ and $Cd_{1-x}Zn_xTe$ respectively. These alloys give advantage of variable bandgap by varying Zn concentration in the alloys. A new structure of TCO/ZnO/$Cd_{1-x}Zn_xS$/$Cd_{1-x}Zn_xTe$/Cu_2Te/Ni is proposed, which can easily be achieved by replacing S by Te during various fabrication processes. Numerical analysis was performed with AMPS 1D software and an efficiency of 24.643% was achieved through bandgap engineering, which is higher than the conventional CdS/CdTe solar cell. The solar cell was also found to be stable at higher temperature.

A modified solar cell structure was proposed, consisting of TCO/ZnO/$Cd_{1-x}Zn_xS$/$Cd_{1-x}Zn_xTe$/Cu_2Te/Ni in which alloy composition was varied in the window layer for achieving a better windowing effect that gives better J_{sc}. But it was accompanied by detrimental V_{oc} and FF, which were then improved by varying alloy composition in the absorber layer which improved lattice matching. A small range of Zn x% around x = 0.2 was found, when the proposed two-fold treatment eventually yielded a better efficiency of 24.643%. The lattice mismatching of modified $Cd_{0.8}Zn_{0.2}S$ /$Cd_{0.8}Zn_{0.2}Te$ was found to be 10.16%, which resembles the original CdS/CdTe lattice mismatch. However, this structure yielded better J_{sc} and V_{oc}, which ultimately resulted in a high efficiency solar cell. The cell also showed very good temperature stability, giving an efficiency gradient of $0.05\%/C^0$.This study shows that careful modification of bandgaps of window and absorber layer can yield better efficiency.

Chapter 1- Introduction

1.1 Research Introduction

Photovoltaic (PV) is a solar electricity which uses semiconductor materials to convert sunlight directly into electricity. PV has enjoyed extraordinary growth during the last few years. This growth can be attributed to some of the advantages solar cell enjoys, such as, low operation cost, environment friendliness, high reliability, modularity, low construction cost and few more.

A general classification of modern day solar cell is shown below:

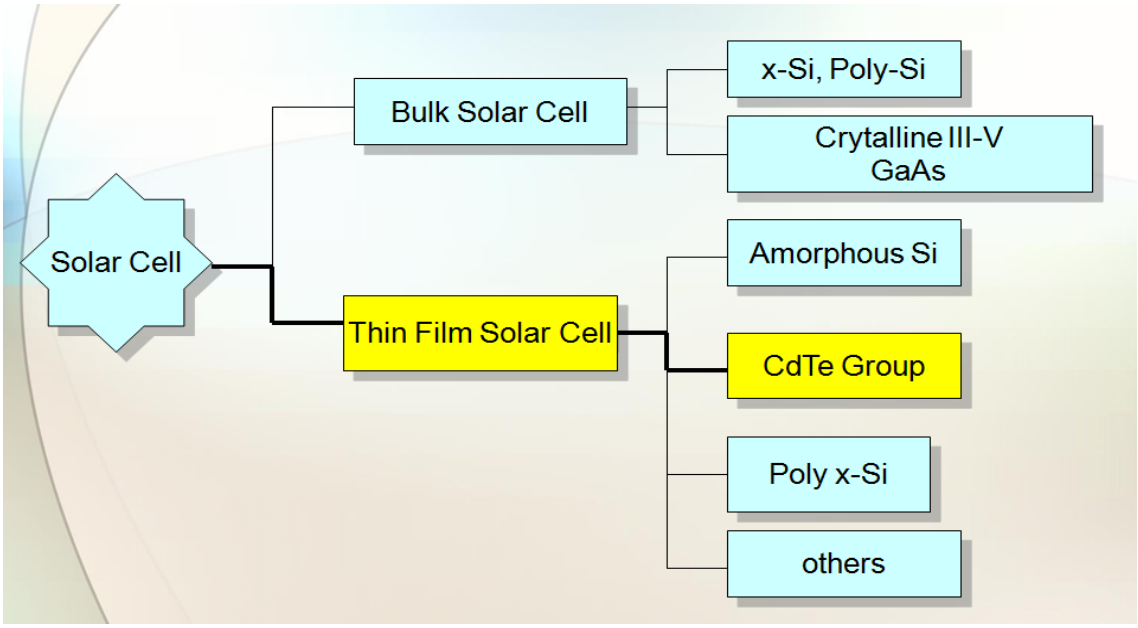

Fig. 1.1 General solar cell classification.

Thin film solar cell is gaining more focus in recent years due to obvious manufacturing cost issues. Particularly CdTe solar cell demands more attention than its counterparts because of some unique advantages this solar cell possesses, namely,high efficiency, cost effectiveness, ability to be bulk produced and openness to wide fabrication procedures such as close-space sublimation (CSS), chemical vapour deposition (CVD), chemical bath deposition (CBD), and sputtering .

This solar cell is also preferable as reduced material is needed because of a high absorption coefficient of $5x10^{15}$/cm of CdTe which indicates that thickness of only a few micron is enough to absorb almost 99% of incident photons having energy greater than bandgap. This result in lesser time spent and ultimately lesser fabrication and manufacturing cost.

1.2 Research Motivation

Modern CdS/CdTe solar cell possesses some deficiencies which have prevented it to reach its theoretical maximum efficiency goal of almost 29%. The realizable efficiency attained so far is just over half of that (16.5%) in laboratory condition. So emphasis must be given in tackling these issues that limit modern CdTe solar cell efficiency.

In this thesis two fundamental problems relating to two core layers (window layer and absorber layer) of a conventional CdTe solar cell structure are addressed, namely-

1. Relatively lower bandgap of window layer (CdS with 2.42 eV).
2. High lattice mismatch between window and absorber layer (10% between CdS and CdTe).

With an attempt to counter these obstacles, a modified solar cell consisting of TCO/ZnO/$Cd_{1-x}Zn_xS$/$Cd_{1-x}Zn_xTe$/Cu_2Te/Ni structure was proposed, instead of the starting cell structure of TCO/ZnO/CdS/CdTe/Cu_2Te/Ni.

1.3 Research Objective

This thesis proposes some modifications in the conventional CdTe solar cell to improve its efficiency and come as close as possible to the theoretical maximum efficiency of 29% for CdTe solar cells. CdTe solar cells have CdTe (p type semiconductor) as absorber or base layer and usually employ CdS (n type semiconductor) as window layer. This p-n junction is actually the core or building block of a solar cell. In practical, some other layers are necessary

for functioning solar cell. Contact layers, TCO, buffer, BSR are some of these subsidiary layers which also play crucial role in the functioning and stability of a solar cell.
This thesis proposes replacing both absorber and window layer of the conventional structure with ternary compound materials in an attempt to find solutions to two important drawbacks of conventional CdTe/CdS solar cell. CdS has a lower bandgap as a window layer material and thus replaced by CdZnS in the proposed design to attain a higher bandgap that might result in more photon current. CdTe was replaced by CdZnTe, another ternary compound to reduce lattice mismatching between CdS and CdTe which degraded cell performance rigorously. The primary focus was on core layers, that is window and absorber layer to increase cell performance in terms of key output parameters such as efficiency, open circuit voltage (Voc), short circuit current density (Jsc) and fill factor (FF).

1.4 Research Outlines

Two-fold approach has been employed in this study-firstly, replacing conventional window layer CdS with tertiary compound CdZnS whose bandgap along with other characteristics are changeable between its two binary constituents CdS and ZnS by changing the alloy composition in $Cd_{1-x}Zn_xS$. The objective is to attain a larger bandgap than existing 2.42 eV to allow photons of maximum possible wavelength through.

Secondly, conventional absorber layer CdTe will be replaced with another ternary compound $Cd_{1-x}Zn_xTe$ to utilize variation in different parameter"s value by changing alloy composition. This time the objective is to improve the existing poor lattice mismatch (almost 10%) between window and absorber layer.

An important fact to be acknowledged is that, changing alloy composition not only change bandgaps but possibly other parameters such as permittivity, lattice constants, carrier mobility, work function too. Each parameter has different effect with different magnitude on the overall solar cell performance. Hence, to investigate the complex effect of alloy composition change, analytical modelling is necessary. AMPS 1D software is utilized in this study to meet that necessity.

Firstly, batch of simulations will be run for $Cd_{1-x}Zn_xS$ /CdTe. The study is to investigate the effect of varying alloy composition in $Cd_{1-x}Zn_xS$ absorber layer on Short circuit current (Jsc) and overall cell efficiency. A better Jsc is expected through optimum manipulation of alloy composition

Secondly, batch of simulations will be run for $Cd_{1-x}Zn_xS$ (modified)/$Cd_{1-x}Zn_xTe$. The study is to investigate the effect of varying alloy composition in $Cd_{1-x}Zn_xTe$ absorber layer on a particular modified $Cd_{1-x}Zn_xS$ (for example x=0.2) window layer with improved bandgap and Jsc.

The expected outcome is an improved lattice matching by varying Zn concentration x% of $Cd_{1-x}Zn_xTe$ can improve the efficiency of the cell with a modified window layer.

1.5 Novelty in the Work

In this work, a new structure of CdS/CdTe based solar cell is proposed, where two of the fundamental drawbacks of traditional CdS/CdTe are addressed. The relatively low bandgap of CdS window layer, along with a significant lattice mismatch between CdS and CdTe lower the efficiency of conventional CdS/CdTe solar cell. This work proposes a novel structure where both window (CdS) and absorber (CdTe) layer are replaced by two II-VI ternary alloys, namely, $Cd_{1-x}Zn_xS$ and $Cd_{1-x}Zn_xTe$ respectively. In previous literatures only one layer (window or absorber) was modified with ternary compounds at a time but not both simultaneously replaced [15, 37]. This thesis introduces both window and absorber layer composition modification simultaneously. These alloys give advantage of variable bandgap by varying Zn concentration in the alloys. A new structure of TCO/ZnO/$Cd_{1-x}Zn_xS$/$Cd_{1-x}Zn_xTe$/Cu_2Te/Ni is proposed, which can easily be achieved by only changing S to Te during various fabrication processes. Numerical analysis was performed with AMPS 1D software and an efficiency of 24.643% was achieved through bandgap engineering, which is higher than the conventional CdS/CdTe solar cell. The solar cell was also found to be stable at higher temperature.

Chapter 2- Background and Motivations

2.1 Solar Cell History

Solar cells are semiconductor devices which convert incident light into electricity by the absorption of photons and subsequent generation of electron-hole pairs. This effect of electricity generation from light absorption, which is known as the photovoltaic effect, was first observed by the French physicist A. E. Becquerel in 1839 [1]. The first solid-state photovoltaic cell was built many years later, by Charles Fritts, in 1883. He coated Selenium (Se) with an extremely thin layer of gold to form the junction. The photovoltaic device was less than 1% efficient [2]. The first practical photovoltaic cell was developed in 1954 at Bell Laboratories [3] by the three scientists- Daryl Chapin, Calvin Souther Fuller and Gerald Pearson. They used a diffused Silicon p-n junction that achieved 6% efficiency.

At present, solar cells are built with many different technologies, and the efficiency level that these devices can achieve is pretty good. In today"s world, we have bulk Si solar cells, we have thin film solar cells fabricated from Si or CdTe, we have dye-sensitized solar cells, and so on. There are even more advanced concept solar cells like Quantum Dot (QD) solar cells, hot carrier solar cells etc. Today, solar cells are used for mass generation of electricity. The added advantage of solar power plants is that they require minimum maintenance, and the input energy is clean and free.

2.1.1 Principle of Operation

Figure 2.1 presents a simplified diagram [4] of a solar cell that utilizes a single p-n junction. With no voltage applied to this junction, an electric field exists in the depletion region of the p-n junction. A simple diagram shows the p-n junction at work which is the fundamental concept of a solar cell.

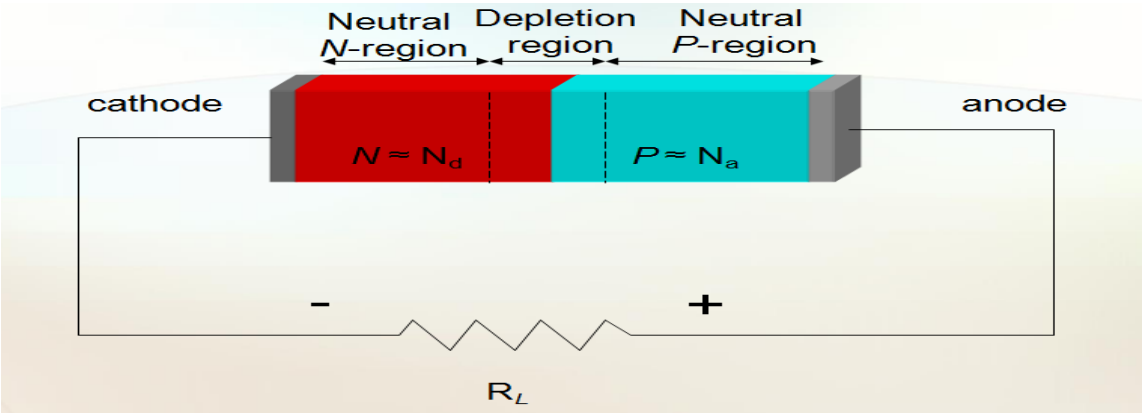

Fig. 2.1 Operation of a p-n junction

For simplicity, we consider that a resistive load is connected with the device. Now, photons incident on the device can create electron-hole pairs in the space-charge region, which are forcibly swept out of the depletion region by the built-in electric field, as the depletion region must be depleted of free charges. This swept out carriers produce a photocurrent I_L, in the reverse-bias direction for the p-n junction. Now, the photocurrent I_L produces a voltage drop across the resistive load, which forward biases the p-n junction. This forward bias produces a forward current, I_F, in the forward-bias direction for the p-n junction. The net current, I, in the reverse bias direction for the p-n junction, is given by equation (1). Fig. 2.2 shows a simplified schematic diagram of a solar cell.

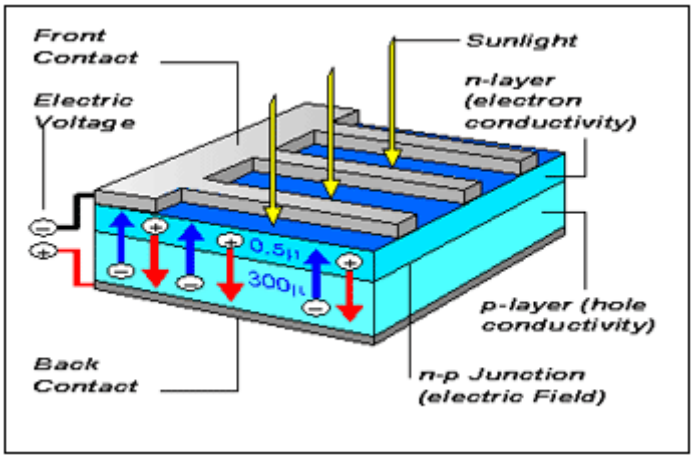

Fig. 2.2 Schematic diagram of a simplified back contact solar cell (image courtesy: ECN, the Netherlands).

$$I = I_L - I_F = I_L - I_S\,[\exp(qV / nkT) - 1] \qquad (1)$$

Where,

n = Ideality factor (taken as 1)

k= Boltzmann constant

T= Temperature in K

q = charge of an electron

I_S = saturation current

2.1.2 Important Quantities

Now, there are two quantities of practical interest, the short-circuit current (I_{sc}) and the open-circuit voltage (V_{oc}). The short-circuit condition occurs when the resistive load is zero, so that V= 0. In this case, I_F is zero, and the short-circuit current, I_{sc}, is given by equation (2).

$$I_{sc} = I_L \qquad (2)$$

Open-circuit condition occurs when the load resistance is infinity. The net current is zero in this case, which finally gives the expression of the open-circuit voltage, V_{oc}, as shown in equation (3).

$$V_{oc} = (nkT / q) \ln (1 + (I_L / I_S)) \qquad (3)$$

It is to be noted that at both short-circuit and open-circuit condition, the power output of a solar cell is zero. Actually, there is a maximum power point on the I-V characteristics graph of a solar cell where $\frac{\partial P}{\partial V} = 0$ (P is the output power). This point is called the maximum power point. The maximum output power, P_m, is given by,

$$P_m = V_m I_m \qquad (4)$$

Where,

V_m= Voltage at Maximum Power Point

I_m = Current at Maximum Power Point

Now, a quantity, termed as „Fill Factor", is used to measure the „squareness" of the I-V curve of a solar cell. This is the ratio of the maximum output power, P_m, to the product of short-circuit current (I_{sc}) and the open-circuit voltage (V_{oc}). Fill factor is commonly abbreviated as FF. A higher FF is desirable, since it increases the maximum output power.

The theoretical FF from a solar cell can be determined by differentiating the power from a solar cell with respect to the voltage and finding the voltage value for which the derivative equals to zero. This is the voltage corresponding to the maximum power point, which is denoted by V_m. An equation involving V_m is given in (5).

$$V_m = V_{oc} - [(nkT / q) \times [ln(qV_m / nkT) + 1] \quad (5)$$

Solving equation (5) by iteration gives the value of V_m. Now, determining the value of I_m requires the knowledge of I_L and I_S. So, this method does not give a closed form solution for determining the maximum output power P_m, the knowledge of which is required for determining FF. So, for all the simulations in our work, we have used the formula (5) given by equation (6) for the calculation of FF.

$$\boldsymbol{FF = \frac{Vocn - ln(Vocn + 0.72)}{Vocn + 1}} \quad \textbf{(6)}$$

Where,

$$\textbf{Vocn = (q/nkT) Voc} \quad \textbf{(7)}$$

Here,

V_{oc}= Open-circuit voltage (in Volt)

n = Ideality factor

q= Charge of an electron = 1.6×10^{-19} Coulomb

K= Boltzman Constant

T= Temperature in K

For all the simulations, we have considered n=1, and T = 300K. The energy conversion efficiency of a solar cell, η, is given in (8).

$$\boldsymbol{\eta = \frac{Voc \times Isc \times FF}{E \times A} \times 100\%} \quad \textbf{(8)}$$

Here,

Isc= Short-circuit current (in Amperes)

FF= Fill Factor

E= Solar irradiance (in W/cm^2)

A= Area of the solar cell (in cm^2)

Now, Isc/Acan be termed as Jsc, which is the short-circuit current density (in A/cm2). So, equation (8) can be rewritten as,

$$\eta = \frac{Voc \times Jsc \times FF}{E} \times 100\% \quad \textbf{(9)}$$

Where,
Jsc= Short-circuit current density (in A/cm^2)

We are considering the use of the solar cell for terrestrial applications. So, to account for the incident sunlight, AM1.5G illumination was considered in the simulation code, as this is the standard terrestrial illumination. According to this, the solar irradiance, E, is taken to be 1000 W/m^2, or, 0.1 W/cm^2. It was also considered that the device is working under 1 sun i.e. no concentrator is used. Using Equation (9), the energy conversion efficiency was calculated.

2.2 Heterojunction Solar Cells

A heterojunction is a p-n junction formed between two different semiconducting materials. Heterojunctions have got numerous applications in optoelectronic devices [6]. Heterojunction solar cells generally employ a p-n or p-i-n structure. In the simplified p-n structure, one material essentially works as an absorber, while the other can be a window layer, or another absorber [7]. The absorber is the functioning layer for optical absorption and generation of electron-hole pairs. The window layer is usually a high bandgap material which is highly transparent to light, so that it can allow almost all the incident photons to reach the absorber.

Heterojunction devices have an inherent advantage over homojunction devices, which require materials that can be doped both p- and n-type. Many semiconducting materials can be doped either p-type or n-type, but not the both. Heterojunctions do not suffer from this limitation. So, many promising materials with good optical absorption capabilities can be investigated to produce optimal cells [8].

Again, a high-bandgap window layer reduces the cell's series resistance, and improves the output voltage [8]. It also helps to reduce recombination of minority carriers at the metal-semiconductor interface around the contacts [9].

For solar cells and other optoelectronic components, it is not sufficient to choose materials with suitable bandgap values and bring them to form a junction. It is also important to make sure that the chosen materials form a junction such that the interface is as much free of energy states in the forbidden band as possible, in order to prevent additional recombination of carriers and carrier trapping [9]. Material combinations satisfying such conditions are not very common. However, many combinations of III-V and II-VI compounds, especially the ternary compounds, satisfy these criteria to large extents [9].

2.3 Silicon Alloys or II-VI Materials – which one is a better choice for Heterojunctions?

Heterojunction solar cells involving Si and Si alloys have been thoroughly investigated [10]. But from a fundamental standpoint, Si is not a very good choice. Its bandgap is lower than the optimum bandgap required for achieving the highest level of efficiency. For terrestrial applications, the optimum bandgap of the absorber should be around 1.4 eV [11], while Si has an indirect bandgap of 1.12 eV. Besides this, Si has low optical absorption coefficient, compared to the high optical-absorption-compounds [12].

Now-a-days, II-VI compounds have gained considerable interest as constituents of both single-junction and multijunction solar cells. The special advantage that these materials offer is their wide range of variation in bandgaps. Besides this, they have got high optical absorption properties, along with high electron mobility and high minority carrier lifetime. They also provide numerous options for proper lattice matching between the heterojunction materials. So, photovoltaic cells fabricated from II-VI compounds typically provide high output current and high efficiency. II-VI ternary and quaternary alloys can offer yet more flexibility, as their bandgaps and other properties can be finely tuned by changing the alloy composition.

2.4 CdTe Solar Cell

CdTe solar cell is one of the most popular thin film solar cells up to date. Its popularity is mainly contributed by its high efficiency, cost effectiveness, ability to be bulk produced and openness to wide fabrication procedures such as close-space sublimation (CSS), chemical vapour deposition (CVD), chemical bath deposition (CBD), and sputtering [13]. A high absorption coefficient of $5x10^{15}$/cm of CdTe indicates that thickness of only a few micron is enough to absorb almost 99% of incident photons having energy greater than bandgap [14]. This reduces the material needed, time spent and ultimately, the fabrication and manufacturing cost.

Despite being one of the most promising pair, CdS/CdTe solar cell has its own deficiencies, which have prevented itself from reaching its theoretical maximum efficiency goal of almost 29%. The realizable efficiency attained so far is just over half of that (16.5%) in laboratory condition in 2004[14]. So, emphasis must be given in tackling these issues that limit modern CdTe solar cell efficiency. This study aims to address two of the most crucial issues of such, namely, the relatively low bandgap of CdS window layer, which absorbs some of the smaller-wavelength incident photons, thus lowering quantum efficiency, and a large lattice mismatch(almost 10%) between CdS and CdTe, which lowers the efficiency significantly along with other fabrication related problems. The bandgap of $Cd_{1-x}Zn_xS$ varies between 2.42 eV (CdS) and 3.6 eV (ZnS). The ternary n-type $Cd_{1-x}Zn_xS$ compounds have been used as a window layer to form heterojunction solar cell with different p-type materials such as CdTe [15-20], Si [21], Cu_xS [22], $CuInSe_2$ [23], $CuGaSe_2$ [24], $Cu(In,Ga)Se_2$ (CIGS) [25]. However the CdS window layer has a lower bandgap, which causes considerable absorption in the short-wavelength region (below 500 nm). To maximize the blue response in CdS/CdTe solar cell, developing an alternative window layer with a higher band-gap is a promising approach. In this study, $Cd_{1-x}Zn_xS$ has been substituted for CdS, as it can provide a more transparent window in the short-wavelength region. It has been demonstrated by Oladeji et al. [20] and several other researchers [26, 27] that the spectral response in the blue region (400-600 nm wavelength region) can be significantly improved using $Cd_{1-x}Zn_xS$/CdTe cell structures. Moreover, $Cd_{1-x}Zn_xS$ films can be deposited in various ways: Vacuum evaporation [28], metal organic chemical vapor deposition (MOCVD) [29], spray pyrolysis [30], successive ionic absorption and reaction (SILAR) [31], photochemical deposition [32] and chemical bath deposition [33]. The publication of Yin et al. [30] reported on $Cd_{1-x}Zn_xS$/CdTe junctions, in which the Zinc concentration was chosen to be around 10%. Oladeji‟s et al. [20]

showed improved Quantum Efficiency (QE) compared to CdS device. The goal of this study is to investigate the effect of bandgap engineering in both window and absorber layers. It is to be noted that changing alloy compositions not only changes bandgaps, but other material properties as well, such as lattice constant, dielectric constant, electron affinity and mobility. Some of them such as lattice constant change linearly with mole fractions following Vegard‟s law, according to which

$$a0.Cd_{1-x}Zn_xS = x.a0.ZnS + (1 - x).a0.CdS.$$

Where a0 is lattice constant, and some of them vary quadratically, such as, modified bad gaps follow the expression-

$$E_g(Cd_{1-x}Zn_xS) = 2.566 + 0.041x + 1.086x^2(eV).$$

Primary objective in window layer is to attain a higher bandgap through changing Zinc concentration. But as stated earlier, changing bandgaps changes other parameters, which can have detrimental effect on overall cell efficiency, despite gaining higher bandgap. One such obvious issue is with lattice constant. The 5.8 Å lattice constant of CdS is already creating almost 10% lattice mismatch with CdTe whose lattice constant is 6.48 Å. Increasing window bandgap also comes with decreased lattice constant aiming towards the lattice constant of ZnS (5.42 Å) which creates further lattice mismatch with CdTe. This explains the second objective of this study, which is to engineer the bandgap of the new absorber ($Cd_{1-x}Zn_xTe$),whose bandgap varies between 2.42 eV (CdS) and 3.6 eV (ZnS). The ternary p-type $Cd_{1-x}Zn_xTe$ compound serves dual purposes. Firstly, it increases slightly the existing bandgap of CdTe (1.45 eV) to a more optimal one and secondly, it improves the lattice matching through shifting towards a lesser lattice constant of ZnTe (6.1 Å) which yields a better lattice matching between window and absorber layer. $Cd_{1-x}Zn_xTe$ as absorber was used at Imamzai et al [36]. Numerical modelling of polycrystalline thin-film solar cells is an important and fruitful strategy to investigate the viability of proposed physical structure, predicting the effect of variations in material properties and geometry on cell performance**,** and correlating of numerical modelling output to experimental results. Numerical simulations for solar cells in AMPS 1D software are done through solving the basic equations related to semiconductors like Poisson‟s equation, continuity equations for free electrons and free holes, etc. Given the complex nature of $Cd_{1-x}Zn_xS/Cd_{1-x}Zn_xTe$ thin film polycrystalline solar cells, the need for

numerical modelling is apparent. Many researchers have carried out simulations with CdTe based solar cells, and a list can be found in the references given in the review by M. Burgelman et al. [34].

2.5 Drawback of II-VI Solar Cells

The problem associated with II-VI solar cells is that these cells are very expensive, compared to the commonly used terrestrial solar cell technologies [37]. This is mainly due to the high fabrication cost of II-VI materials, along with the unavailability of necessary fabrication technology in few cases. So, the use of II-VI solar cells is still limited to applications, where the efficiency is prioritized over the cost [38, 39]. Utilization of such solar cells for general terrestrial applications requires reduction of materials processing and fabrication costs. Another way to address this problem is to use concentrators with solar cells. Concentrated solar cells can give up to 2000 times the power output of a solar cell working under 1 sun, depending on the concentration level. Though concentrators are very expensive, they can offer a good trade-off between the PV system cost and the achievable high efficiency [40-42].

2.6 About the Software

Investigating the complex effect of alloy composition change requires analytical modelling. AMPS 1D software is utilized in this study to meet that necessity. AMPS 1D is a one-dimensional computer program for simulating transport physics in solid state devices. It uses the first-principles continuity and Poisson‟s equations approach to analyse the transport behaviour of semiconductor electronic and optoelectronic device structures. These device structures can be composed of crystalline, polycrystalline, or amorphous materials or combinations thereof. This program, called AMPS (Analysis of Microelectronic and Photonic Structures), numerically solves the three governing semiconductor device equations (the Poisson equation and the electron and hole continuity equations) without making any a-priori assumptions about the mechanisms controlling transport in these devices. With this general and exact numerical treatment, AMPS may be used to examine a variety of device structures that include-

- homojunction and heterojunction p-n and p-i-n, solar cells and detectors;
- homojunction and heterojunction p-n, p-i-n, n-i-n, and p-i-p microelectronic structures;
- multi-junction solar cell structures;
- multi-junction microelectronic structures;
- compositionally-graded detector and solar cell structures;
- compositionally-graded microelectronic structures;
- novel device microelectronic, photovoltaic, and opto-electronic structures;
- Schottky barrier devices with optional back layers.

From the solution provided by an AMPS simulation, output such as current voltage characteristics in the dark and, if desired, under illumination can be obtained. These may be computed as a function of temperature. For solar cell and detector structures, collection efficiencies as a function of voltage, light bias, and temperature can also be obtained. In addition, important information such as electric field distributions, free and trapped carrier populations, recombination profiles and individual carrier current densities as a function of position can be extracted from the AMPS program. As stated earlier, AMPS‟ versatility can be used to analyze transport in a wide variety of device structures that can contain combinations of crystalline, polycrystalline, or amorphous layers. AMPS is formulated to analyze, design, and optimize structures intended for microelectronic, photovoltaic, or opto-electronic applications. Fig. 2.3 shows a snapshot of AMPS 1D home screen.

A comparison of AMPS with other known programs shows that AMPS is the only computer modeling program available that incorporates all of the following physics:

- a contact treatment that allows thermionic emission and recombination to take place at device contacts;
- a very generalized gap state model that can fit any density of states distribution in the bulk or at an interface;
- both band-to-band and Shockley-Read-Hall recombination;
- a recombination model that computes Shockley-Read-Hall recombination traffic through any inputted general gap state distribution instead of the often-used single recombination level approach;
- full Fermi-Dirac, and not just Boltzmann, statistics;

- gap state populations computed with actual-temperature statistics rather than the often used T=0K approach;
- a trapped charge model that accounts for charge in any inputted general gap state distribution;
- a gap state model that allows capture cross-sections to vary with energy;
- gap state distributions whose properties can vary with position;
- carrier mobility that can vary with position;
- electron and hole affinities that can vary with position;
- mobility gaps that can differ from optical gaps;
- the ability to calculate device characteristics as a function of temperature in both forward and reverse bias as well as with or without illumination;
- The ability to analyze device structures fabricated using single crystal, polycrystalline, or amorphous materials or all three.While working with this software, values of required material parameters (bandgap, mobility, thickness, doping level etc.) are given as inputs by the user. Devices fabricated from any material, for which these parameters are known, can be modelled by the software.

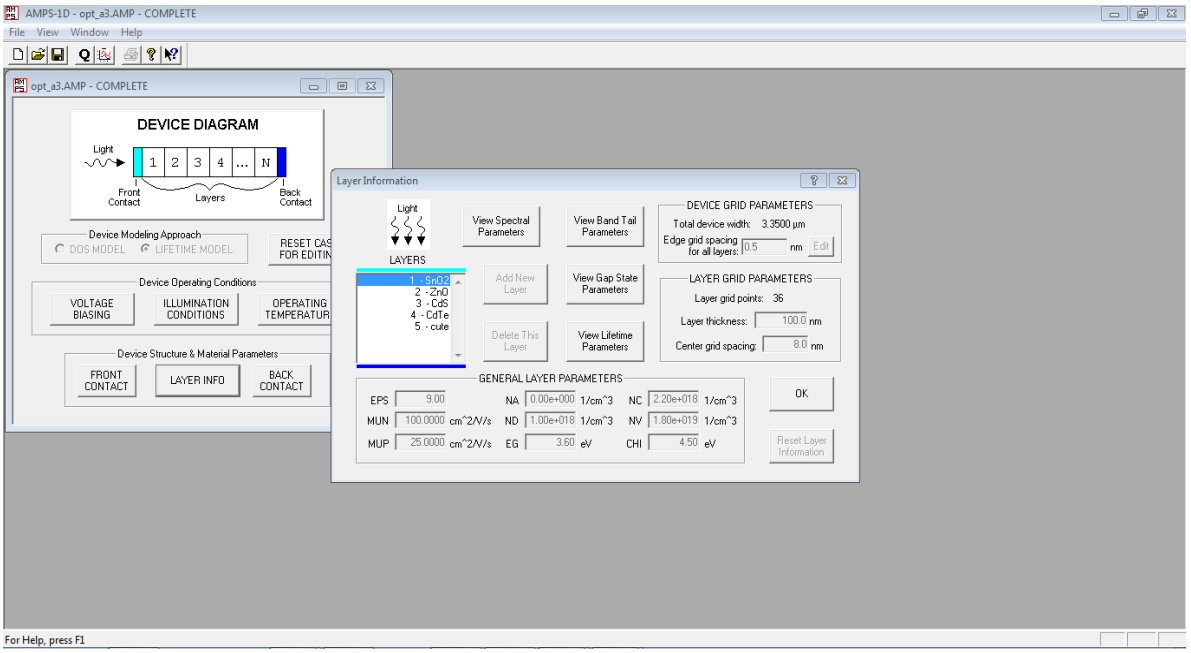

Fig. 2.3 AMPS 1D simulation software.

Chapter 3- Methodology

3.1 Selecting Initial Design

In order to demonstrate the drawbacks of conventional CdS/CdTe solar cell an initial design was chosen which will serve as foundation for the modified structure to be proposed later on. The initial design consists of five layers (exclusive of substrate and contacts) namely; Transparent Conductive Oxide (TCO/ CTO), a buffer layer, a window layer, an absorber layer and a Back Surface Reflector (BSR) layer. For the initial design Tin Oxide (SnO_2) was chosen as TCO, Zinc Oxide (ZnO) was chosen as buffer layer, CdS as window layer, CdTe as absorber and Cu_2Te as BSR. This initial structure of TCO/ZnO/CdS/CdTe/Cu_2Te/Ni shall be the starting point of this thesis.

The schematic structure of the initial design is shown in Fig. 3.1.

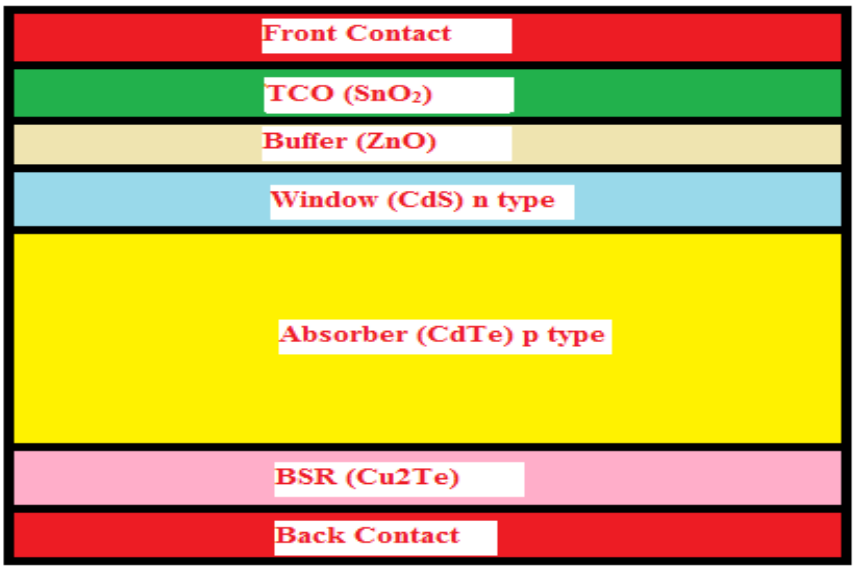

Fig. 3.1 Schematic diagram of the initial CdS/CdTeheterojunction solar cell.

3.1.1 Choice of Layer Materials

For the purpose of simulation in AMPS 1D some key parameters of the layers were to be keyed in. These parameters are to remain unchanged for the future design and simulations unless otherwise specified. Table 3.1 shows the general layer parameters.

Table 3.1

General layer parameters

Parameter	ZnO	n-CdS	p-CdTe	p-Cu_2Te
W (μm)	0.1	0.05	1	0.1
$\varepsilon/\varepsilon_0$	9.0	10	9.4	10
$\mu_c(cm^2/Vs)$	100	340	1050	500
$\mu_p(cm^2/Vs)$	25	50	100	100
n, p (cm^{-3})	10^{18}	10^{16}	5×10^{15}	10^{21}
Eg (eV)	3.35	2.42	1.45	1.18
N_c (cm^{-3})	2.2×10^{18}	2.2×10^{18}	8×10^{17}	7.8×10^{17}
N_v (cm^{-3})	1.8×10^{19}	1.7×10^{19}	1.8×10^{19}	1.6×10^{19}
χ (eV)	4.50	4.4	4.28	4.50

Where,

W = Thickness (μm)

$\varepsilon/\varepsilon_0$ = Relative permittivity

μ_c = Electron mobility (cm^2/Vs)

μ_p = Hole mobility (cm^2/Vs)

n, p = Donor/ Acceptor concentration (cm^{-3})

Eg = Bandgap(eV)

N_c = DOS in Conduction band (cm^{-3})

N_v =DOS in valence band(cm^{-3})

χ = Electron affinity (eV)

3.1.2 Choice of Contact Materials

Nickel (Ni) was chosen as contacts because of its superior performance recently observed as contact layer material.Table 3.2 list the contact parameters used in AMPS 1D for the simulation purpose and will remain unchanged throughout the study for several other simulations to come

Table 3.2

Contact parameters

Parameters	Front contact	Back contact
Φ_b [eV]	Φ_{bn} = 0.10	Φ_{bp} = 1.25
S_e [cm/s]	1×10^7	1×10^7
S_h [cm/s]	1×10^7	1×10^7
R_f [I]	0.01	0.99

Where,

S_e = Surface electron velocity (cm/s)

S_h = Surface hole velocity (cm/s)

R_f = Reflectibilty (0~1)

Φ_b = Barrier hieght (eV)

3.2 First Modified Structure

The first modified structure involves replacing conventional window layer CdS with tertiary compound CdZnS whose band gap along with other characteristics are changeable between its two binary constituents CdS and ZnS by changing the alloy composition in $Cd_xZn_{1-x}S$. The objective is to attain a larger bandgap than existing 2.42 eV to allow photons of maximum possible wavelength through.

3.2.1 Layer Parameters for the First Modified Structure

At the beginning, some default values of contact parameters and general layer parameters for each layer of the device was chosen that are listed in Table 3.3 and 3.4 respectively.

Table 3.3

Contact parameters

Parameters	Front contact	Back contact
Φ_b [eV]	Φ_{bn} = 0.10	Φ_{bp} = 1.25
S_e [cm/s]	1×10^7	1×10^7
S_h [cm/s]	1×10^7	1×10^7
R_f [I]	0.01	0.99

Table 3.4

General layer parameters

Parameter	ZnO	n-$Cd_{1-x}Zn_xS$	p-CdTe	p- Cu_2Te
W (μm)	0.1	0.05	1	0.1
$\varepsilon/\varepsilon_0$	9.0	10-8.5	9.4	10
$\mu_c(cm^2/Vs)$	100	340-165	1050	500
$\mu_p(cm^2/Vs)$	25	50-5	100	100
n, p (cm^{-3})	10^{18}	10^{16}	5×10^{15}	10^{21}
Eg (eV)	3.35	2.42-3.7	1.45	1.18
N_c (cm^{-3})	2.2×10^{18}	2.2×10^{18}	8×10^{17}	7.8×10^{17}
N_v (cm^{-3})	1.8×10^{19}	1.7×10^{19}	1.8×10^{19}	1.6×10^{19}
χ (eV)	4.50	4.4-3.9	4.28	4.50

3.2.2 Modelling the Window Layer for the First Modified Structure

In this part of the work, a new window layer material, $Cd_{1-x}Zn_xS$ was introduced that replaced the CdS in the initial design. Next, keeping every other device parameter fixed at some default (initial) value, simulations were run for different value of x (e.g. x=0, 0.2, 0.4, 0.6, 0.8 and 1) and changes in the output characteristics were observed. $Cd_{1-x}Zn_xS$ is ternary II-VI compound comprised of two binary compound CdS and ZnS. So by changing the value of x, each time we get a material that is precise mixture of CdS (for x=0) and ZnS (for x=1).

Simulation was conducted with these default values, and a light J-V characteristics graph was acquired. From the graph, values of open-circuit voltage (V_{oc}), short-circuit current density (J_{sc}), Fill factor (FF) and efficiency (η) were obtained. FF and efficiency can also be calculated using the equations (6) and (9), respectively. This efficiency is the efficiency under standard conditions, mentioned in section 2.1.2.

First batch of simulations was run for $Cd_{1-x}Zn_xS$/CdTe where only window layer was modified by changing Zn concentration x% and all other layers with all their baseline parameters were kept unchanged. Simulations were run for x=0, 0.2, 0.4, 0.6, 0.8, 1.

The objective was to find out and analyse the effect of molar composition in $Cd_{1-x}Zn_xS$ on $Cd_{1-x}Zn_xS$/CdTe solar cell. Changing value of x each time meant having a totally different material altogether with its unique electrical and optical parameters. So six sets of simulations were run for six values of x (x=0, 0.2, 0.4, 0.6, 0.8, 1) keeping all other layer parameters unchanged with careful modification only for window layer, $Cd_{1-x}Zn_xS$ according to different values for x.

3.3 Second modified structure

Secondly, conventional absorber layer CdTe was replaced with another ternary compound $Cd_xZn_{1-x}Te$ to utilize variation in different parameter‟s value by changing alloy composition with an optimal value of x in $Cd_xZn_{1-x}S$ found from first modified structure simulations. This time the objective was to improve the existing poor lattice mismatch (almost 10%) between window and absorber layer.

3.3.1 Layer parameters for the second modified structure

Before conducting simulations, some default values for thickness, doping concentration and alloy composition for each layer were fixed. Table 3.5 and 3.6 summarizes these default values.

Table 3.5

Contact parameters

Parameters	Front contact	Back contact
Φ_b [eV]	$\Phi_{bn} = 0.10$	$\Phi_{bp} = 1.25$
S_e [cm/s]	1×10^7	1×10^7
S_h [cm/s]	1×10^7	1×10^7
R_f [I]	0.01	0.99

Table 3.6

General layer parameters

Parameter	ZnO	n- $Cd_{0.8}Zn_{0.2}S$	p- $Cd_{1-x}Zn_xTe$	p- Cu_2Te
W (μm)	0.1	0.05	1	0.1
$\varepsilon/\varepsilon_0$	9.0	9.4	9.4	10
$\mu_c(cm^2/Vs)$	100	275	1050-340	500
$\mu_p(cm^2/Vs)$	25	24	100	100
n, p (cm^{-3})	10^{18}	10^{16}	5×10^{15}	10^{21}
Eg (eV)	3.35	2.62	1.45-2.25	1.18
N_c (cm^{-3})	2.2×10^{18}	2.2×10^{18}	8×10^{17}	7.8×10^{17}
N_v (cm^{-3})	1.8×10^{19}	1.7×10^{19}	1.8×10^{19}	1.6×10^{19}
χ (eV)	4.50	4.4	4.28-3.5	4.50

3.3.2 Modelling the absorber layer for the second modified structure

In the previous section we discussed about a modified window layer introduced in our initial design to replace original window layer of CdS to improve the bandgap and thus increase carrier current. After the successful completion of that task it is the second drawback of conventional CdTe solar cell that this section aims to encounter. For that purpose, keeping the modified window layer ($Cd_{1-x}Zn_xS$) with the best result (e.g x=0.2) obtained from previous section, a new absorber layer was introduced and analysed in this section. Another ternary compound $Cd_{1-x}Zn_xTe$ replaced original CdTe as the absorber layer to minimize the lattice mismatch between window and absorber layer that was prevalent in the conventional design.

The second batch of simulations conducted in this section was run for $Cd_{0.8}Zn_{0.2}S/Cd_{1-x}Zn_xTe$. The study was to investigate the effect of varying alloy composition in $Cd_{1-x}Zn_xTe$on a particular modified $Cd_{1-x}Zn_xS$ (here x=0.2) window layer with improved bandgap and Jsc. The idea was to observe whether improving the lattice matching by varying Zn concentration x% of $Cd_{1-x}Zn_xTe$ can improve the efficiency of the cell with a modified window layer.

Now, simulations were conducted by varying the value of x for the absorber layer alloy ($Cd_{1-x}Zn_xTe$) from 0 to 1, in steps of 0.2. For each simulation, value of every other device parameter was kept the same as listed in Table 3.5 and 3.6. Now, a light J-V characteristics curve was obtained for every simulation, which provided the energy conversion efficiency, Jsc, Voc and FF for that particular simulation. In this manner, efficiency, Jsc, Voc and FF for each of the simulations was obtained. Then, these output parameters were plotted against x (Zinc mole fraction) for the absorber layer. The efficiency curve, Jsccurve, Voc curve and FF curve were analysed for getting an idea about the optimization of Zinc mole fraction in $Cd_{1-x}Zn_xTe$ for achieving higher efficiency.

Afterwards, through analysing the output parameters with varying x value, an optimum absorber layer was found. Together with the optimum window layer achieved in the last section, section 3.4 discusses the optimum solar cell design this thesis proposes and further aims to analyse the proposed structure against other design variables.

3.4 Optimized structure

From article 3.2 and 3.3 a new solar structure was developed by modifying the window and absorber layer in the initial design of TCO/ZnO/CdS/CdTe/Cu_2Te/Ni. Schematic diagram of the new TCO/ZnO/$Cd_{0.8}Zn_{0.2}S$/$Cd_{0.8}Zn_{0.2}Te$/Cu_2Te/Ni is shown in figure 3.2. In this chapter the proposed solar cell will be investigated against some typical input design parameters such as window thickness, absorber thickness and temperature to further analyse this new design in order to improve its performance in terms of efficiency and stability.

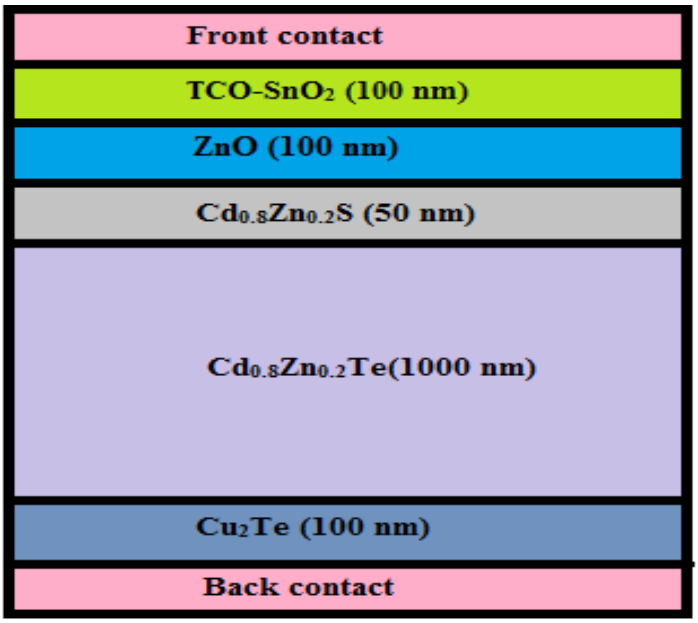

Fig. 3.2 Schematic diagram of the proposed solar cell

3.4.1 Varying window layer thickness of the optimized structure

After achieving an optimized cell design in terms of molar composition in the core layer, next attempts were towards developing this structure by investigating variation of cell performance with varying window layer thickness. The objective was to find a suitable window layer thickness for the purpose of fabrication. The optimum structure of TCO/ZnO/$Cd_{0.8}Zn_{0.2}S$/$Cd_{0.8}Zn_{0.2}Te$/Cu_2Te was simulated across a wide range of plausible window thickness. The simulations were run for window ($Cd_{0.8}Zn_{0.2}S$) thickness ranging from 100 nm to 1000 nm with a step of 100 nm.

3.4.2 Varying absorber layer thickness of the optimized structure

Next, the optimized cell design in terms of molar composition was investigated by observing the variation of cell performance with varying absorber layer thickness. The objective was to find a suitable absorber layer thickness for the purpose of finding out layer information for fabrication. The optimum structure of TCO/ZnO/$Cd_{0.8}Zn_{0.2}S$/$Cd_{0.8}Zn_{0.2}Te$/Cu_2Te was simulated across a wide range of plausible absorber thickness. The simulations were run for absorber ($Cd_{0.8}Zn_{0.2}Te$) thickness ranging from 1 µm to 10 µm with a step of 1 µm.

3.4.3 Varying operating temperature of the optimized structure

Finally, the optimized cell design in terms of molar composition was investigated by observing the variation of cell performance with varying operating temperature. The objective was to investigate temperature stability of the proposed cell structure. So, the optimum structure of TCO/ZnO/$Cd_{0.8}Zn_{0.2}S$/$Cd_{0.8}Zn_{0.2}Te$/Cu_2Te was simulated across a wide range of operating temperature to find out its temperature withstanding ability. The simulations were run for absorber operating temperature ranging from 0 degree centigrade to 100 degree centigrade with a step of 20 degree centigrade.

Chapter 4- Results and Discussions

4.1 The Initial Design

The different results along with discussions of the initial design simulations are presented in the form of J-V curves and spectral response (SR) in the following sections. As already mentioned earlier, the initial design is made of TCO/ZnO/$Cd_{1-x}Zn_xS$/$Cd_{1-x}Zn_xTe$/Cu_2Te/Ni.

4.1.1 J-V curve

Figure 4.1 shows that the initial design yields an open-circuit voltage (V_{oc}) of -0.927 V, and the short-circuit current density (J_{sc}) is 33.064 mA/cm^2. Fill factor (FF) was directly provided by the software but still can be calculated using the formula given in (6). For this simulation, the fill factor was found to be 0.854. This design is already resulting in high efficiency of 23.803% because of advanced layer designs. The introduction of high quality TCO along with buffer and BSR layer make this design a very improved one. But this thesis aims to improve it further by addressing some drawbacks associated with core layers and propose some solutions to overcome it.

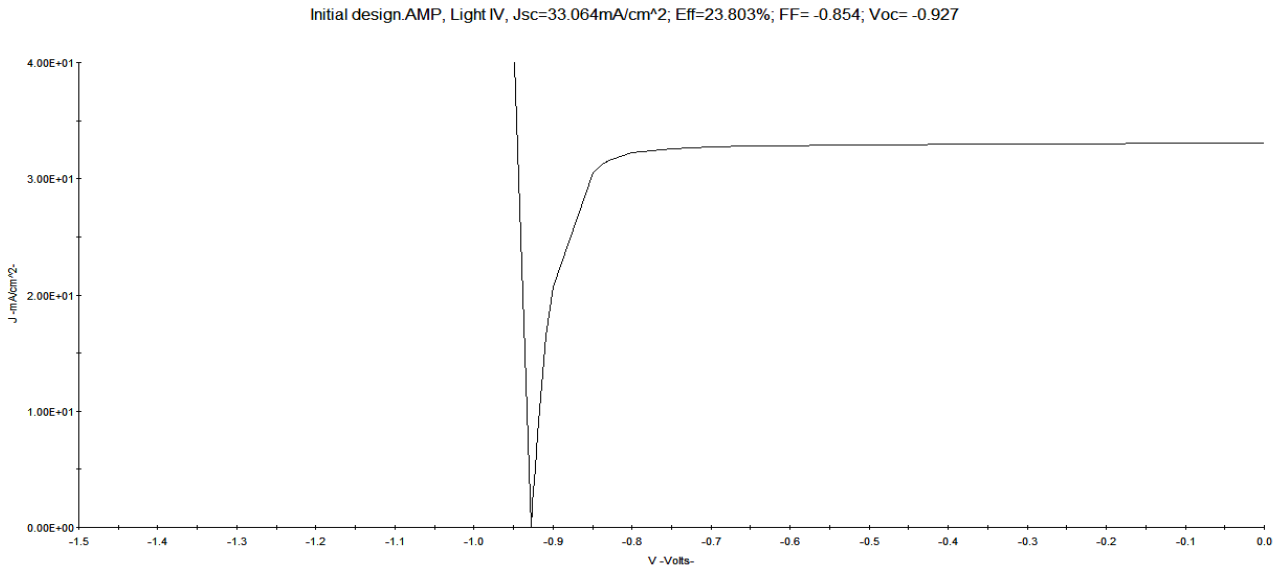

Fig. 4.1 Light J-V curve for the initial design of CdS/CdTe solar cell

The working conditions for the solar cell (solar irradiance, temperature, concentration level) were considered as mentioned in section 2.1.2.

4.1.2 Spectral responses

Subsequently in Figure 4.2 the Spectral Response (SR) of the initial design is shown.

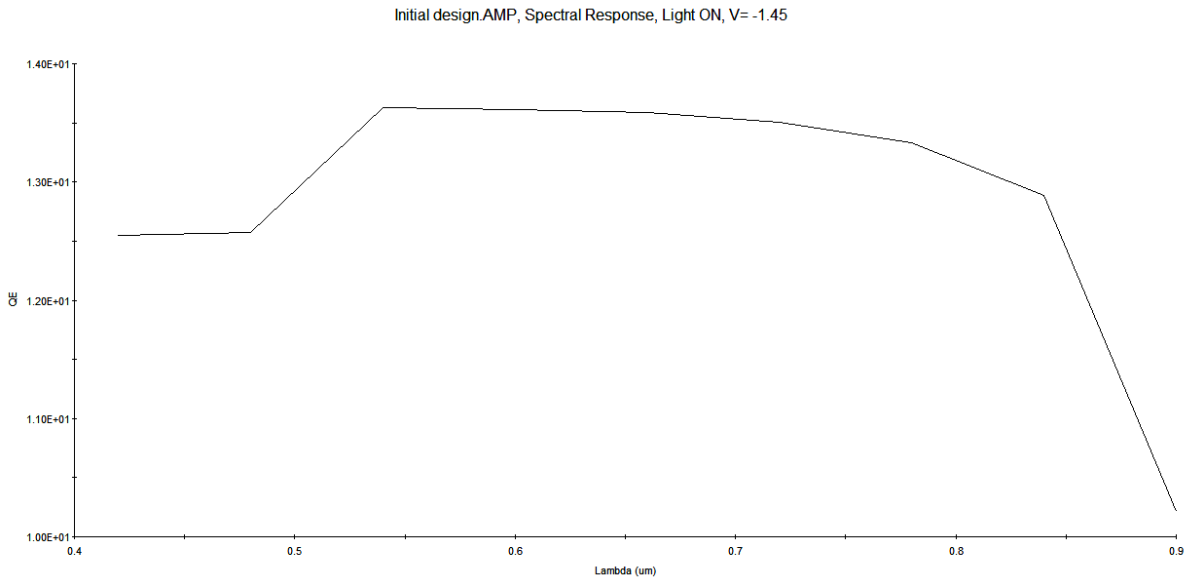

Fig.4.2 Spectral Response (SR) for the initial design of CdS/CdTe solar cell

It is seen from figure that, for the initial design, spectral response (SR) is quite satisfactory giving a flat QE (~1.35e+01) for wavelengths ranging between 550-800 nm. SR can be correlated with the short circuit current density, Jsc. In the proposed design it will be seen that both Jsc and therefore the SR can be improved further by introducing some modifications in the core layers that is the window and absorber layer.

The light J-V characteristics curve and SR of an initial design of the CdS/CdTe heterojunction solar cell has been simulated under AM1.5G illumination with AMPS 1D simulation software. The effect of introducing subsidiary layers such as TCO, buffer and BSR layer on the energy conversion efficiency has been illustrated through the simulation results. Finally, under 1 sun, an energy conversion efficiency of 23.803% has been reported, for the device shown schematically in Figure 3.1.

4.2 First modified structure with modified window layer

Next batch of simulations was run for $Cd_{1-x}Zn_xS/CdTe$ where only window layer was modified by changing Zn concentration x% and all other layers with all their baseline parameters were kept unchanged. Simulations were run for x=0, 0.2, 0.4, 0.6, 0.8 and 1. Figure 4.3 to 4.14 illustrates the findings of the simulations.

As expected, short circuit current increased with increasing Zn concentration, as bandgap was increasing letting more photons of lower wavelength through the device window, although slightly. But with increase of Zn concentration, the lattice mismatch kept increasing too. This increased series resistance and ultimately lowered the fill factor (FF). Moreover increasing Zn concentration also resulted in lower mobility and electron affinity and permittivity which further reduced FF and Voc. Decrease in Voc was less severe compared to FF. Ultimately, despite an improvement in short circuit current, the overall efficiency kept decreasing due decreasing FF and Voc. From the table 4.1 it is quite apparent that the overall performance took a dive for the worse after x=0.6. It was found that 33.109 mA/cm^2 is the highest Jsc, found for x=0.6.

Table 4.1

Simulation Results for Different Alloy Compositions of Cadmium Zinc Sulphur

x in $Cd_{1-x}Zn_xS$	**Energy Gap (eV)**	**Jsc (mA/ cm^2)**	**Voc (V)**	**FF**	**η (%)**
0	2.45	33.064	0.927	0.854	23.803
0.2	2.5	33.083	0.927	0.854	23.815
0.4	2.62	33.1	0.922	0.827	22.935
0.6	2.78	33.105	0.918	0.817	22.563
0.8	2.99	33.095	0.918	0.816	22.533
1	3.24	33.054	0.918	0.711	19.614

4.2.1 Light J-V curves

Figure 4.3-4.8 show the most important output feature of a solar cell, that is, Light J-V curves. AMPS 1D provides a well documented J-V curve which includes key output parameters such as Voc, Jsc, FF and efficiency. Observing the light j-V curve alone can give enough perspective and insight to the solar cell performance. Figure 4.3-4.8 show light J-V curves for $Cd_{1-x}Zn_xS$/CdTe solar cell for different values of x in $Cd_{1-x}Zn_xS$.

Unlike some other software such as ADEPT, the output figures in AMPS 1D includes all necessary output parameters such as efficiency, Voc, Jsc and FF. Specially, in most cases FF has to be calculated from the equation presented in the chapter 2 as it is not often given directly. AMPS 1D directly provides the FF value which makes analysis very convenient and quick. Analysis of the co-dependency of key output parameters to molar variation is described in this section.

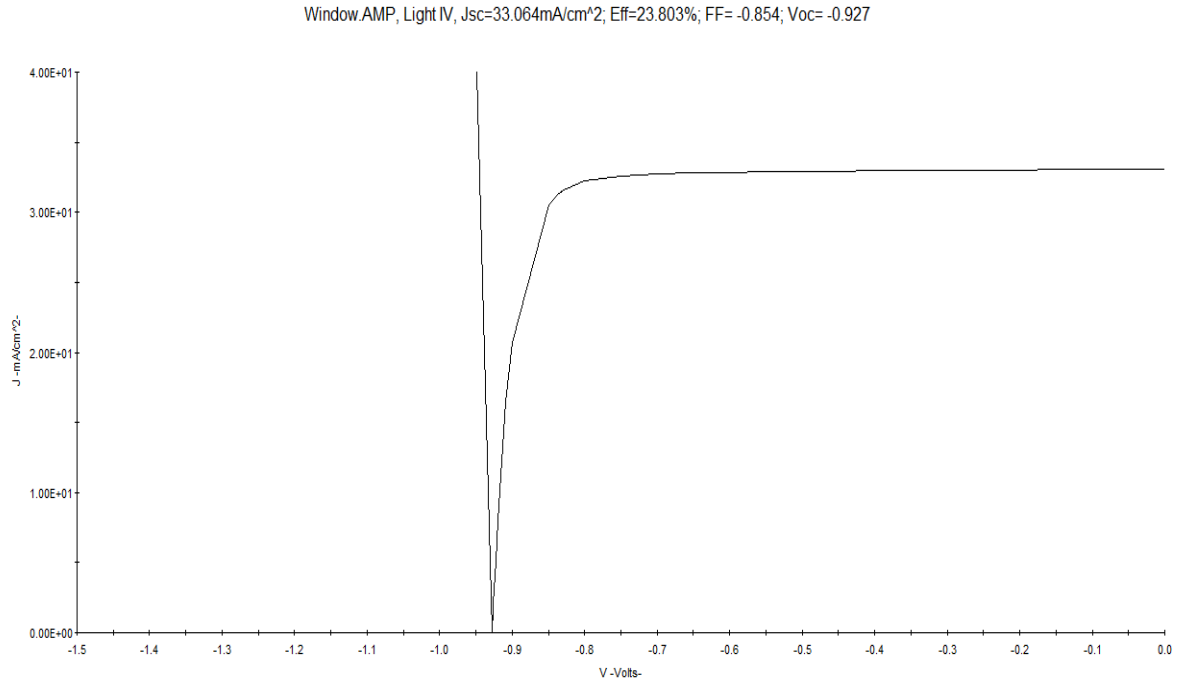

Fig. 4.3 Light J-V characteristics for$Cd_{1-x}Zn_xS$/CdTe solar cell having window layer with x = 0.

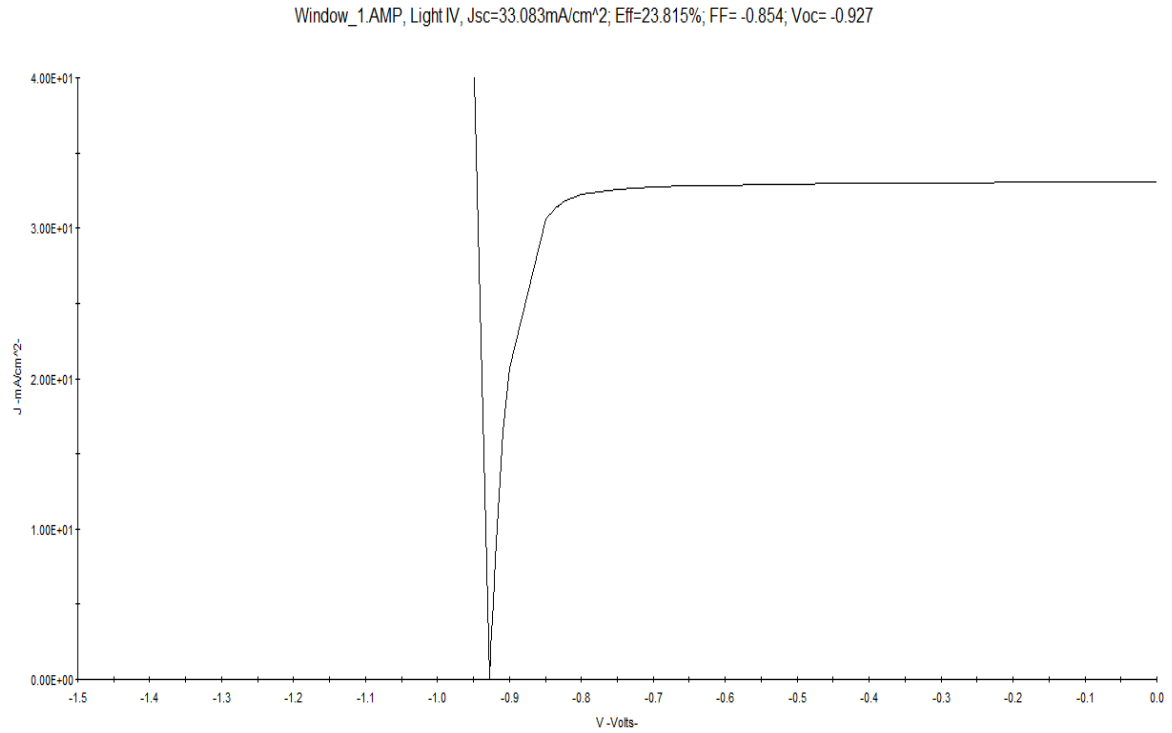

Fig. 4.4 Light J-V characteristics for$Cd_{1-x}Zn_xS$/CdTe solar cell having window layer with x = 0.2

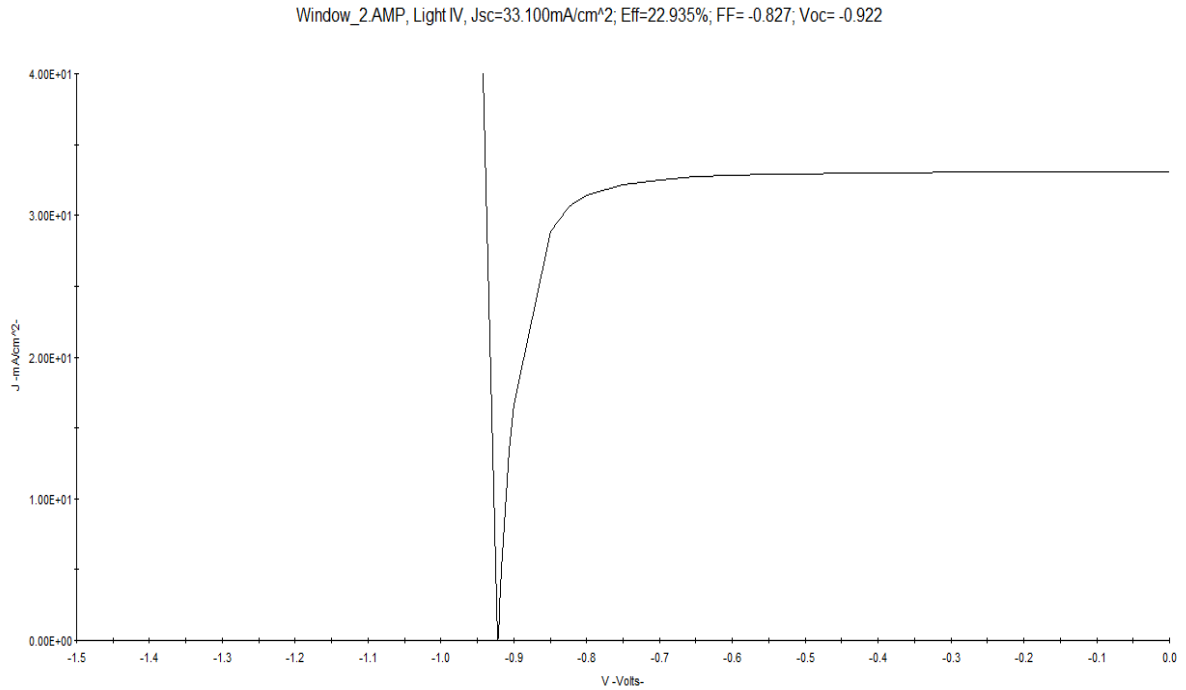

Fig. 4.5 Light J-V characteristics for$Cd_{1-x}Zn_xS$/CdTe solar cell having window layer with x = 0.4

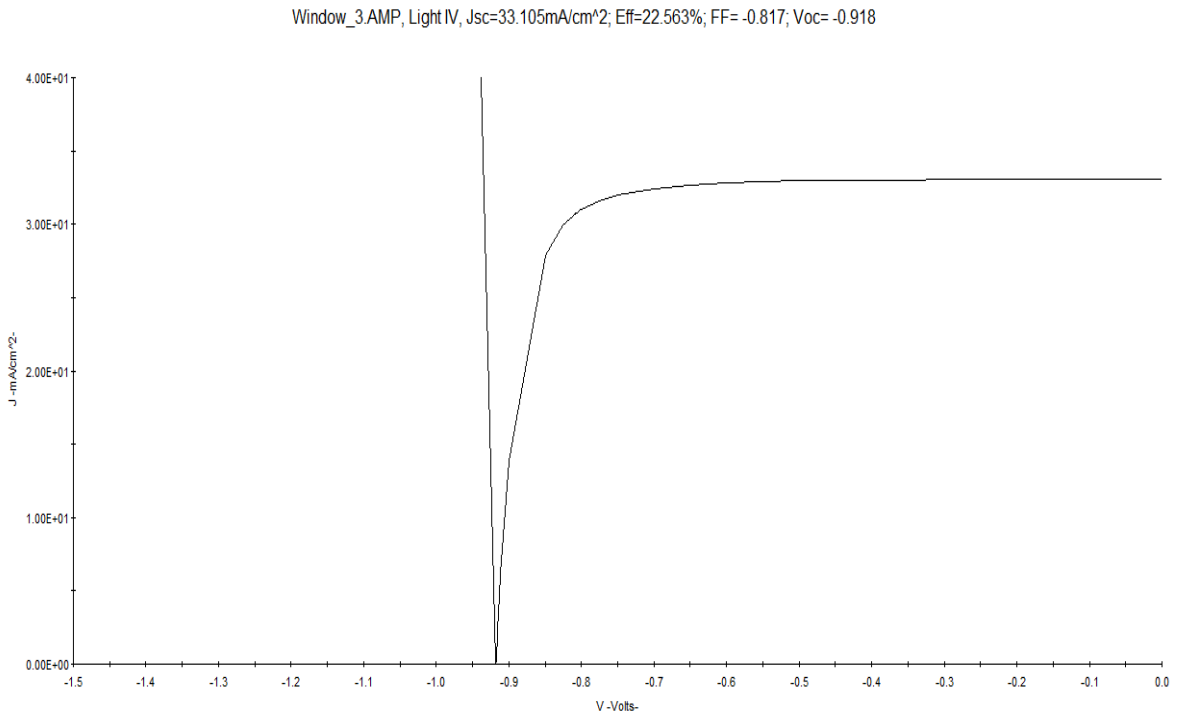

Fig. 4.6 Light J-V characteristics for $Cd_{1-x}Zn_xS/CdTe$ solar cell having window layer with x = 0.6

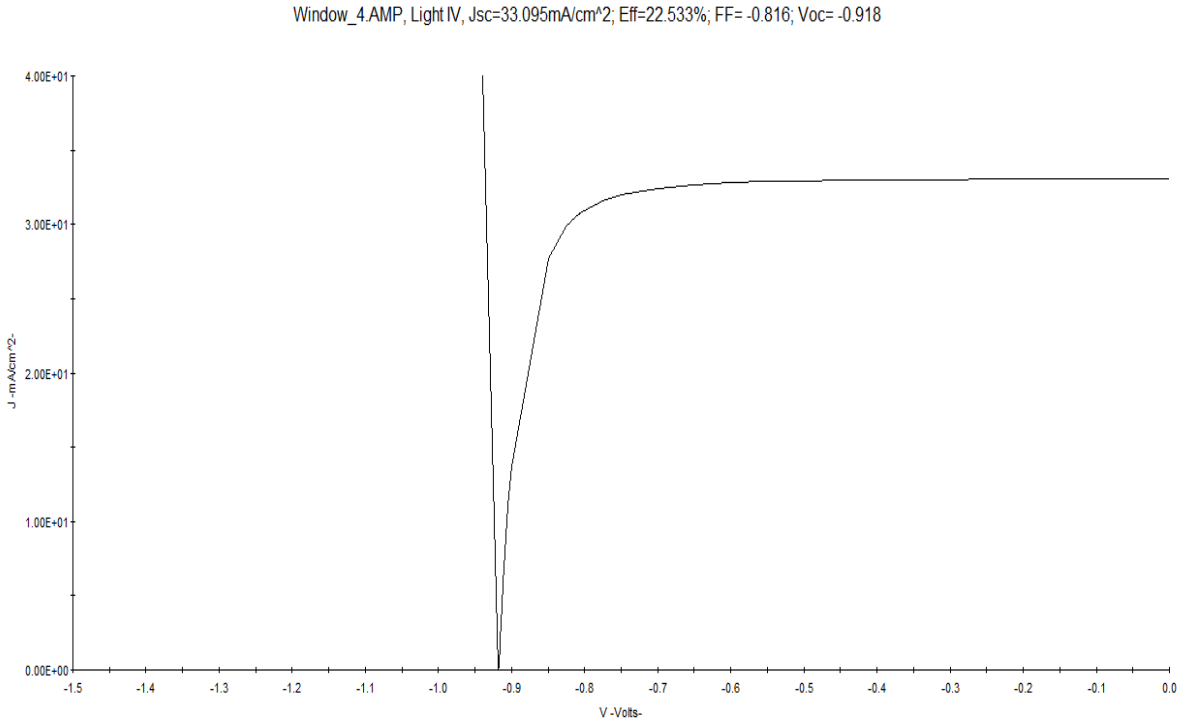

Fig. 4.7 Light J-V characteristics for $Cd_{1-x}Zn_xS/CdTe$ solar cell having window layer with x = 0.8

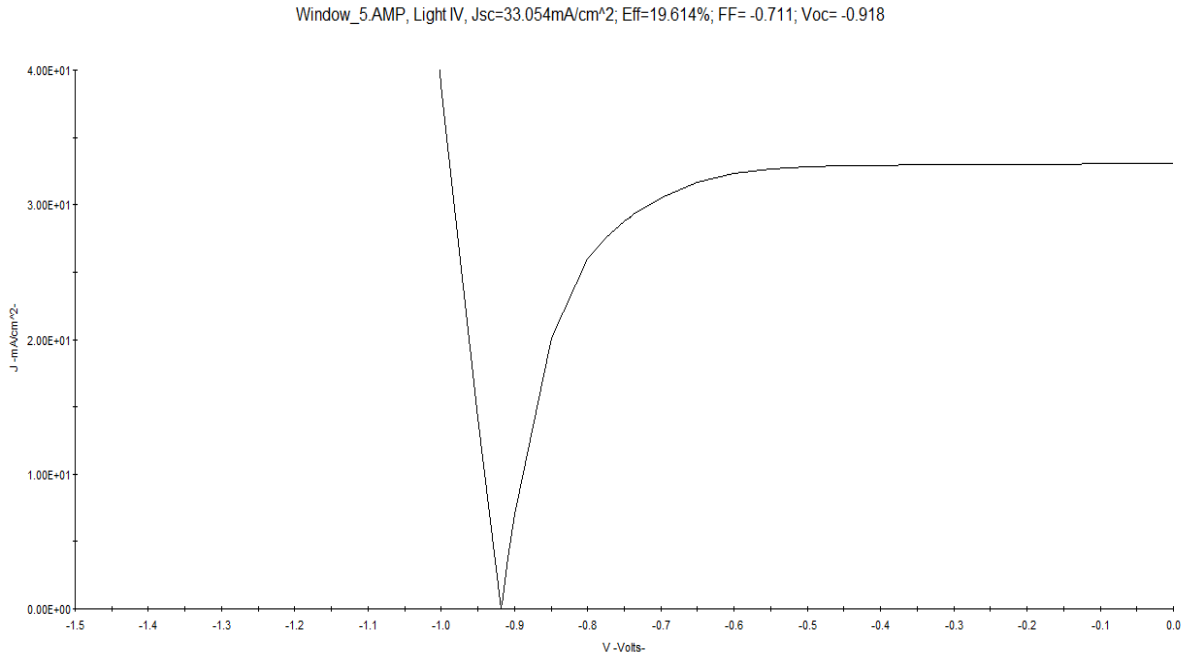

Fig. 4.8 Light J-V characteristics for $Cd_{1-x}Zn_xS/CdTe$ solar cell having window layer with x = 1

4.2.2 Spectral Responses

Spectral response (SR) can provide very important information about a solar cell. Frequency specific conversion of light or photon energy to electrical energy is depicted by spectral response of asolar cell. It is also known as quantum efficiency (QE) curve. Figure 4.9-4.14 shows the spectral response for $Cd_{1-x}Zn_xS/CdTe$ solar cell for different values of x in $Cd_{1-x}Zn_xS$.

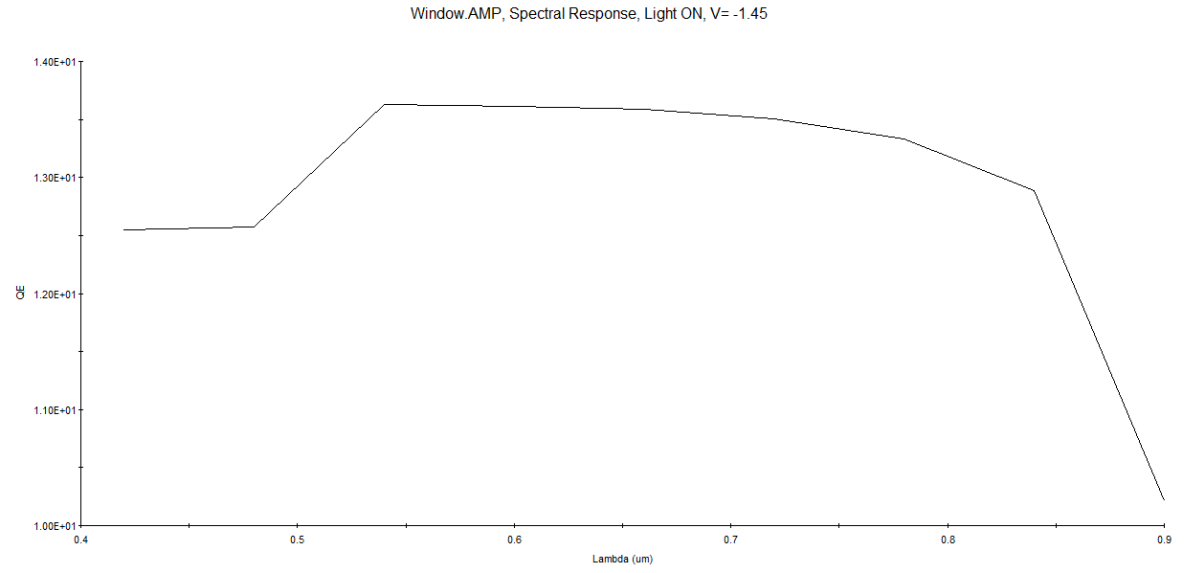

Fig. 4.9 Spectral response for $Cd_{1-x}Zn_xS/CdTe$ solar cell having window layer with x = 0

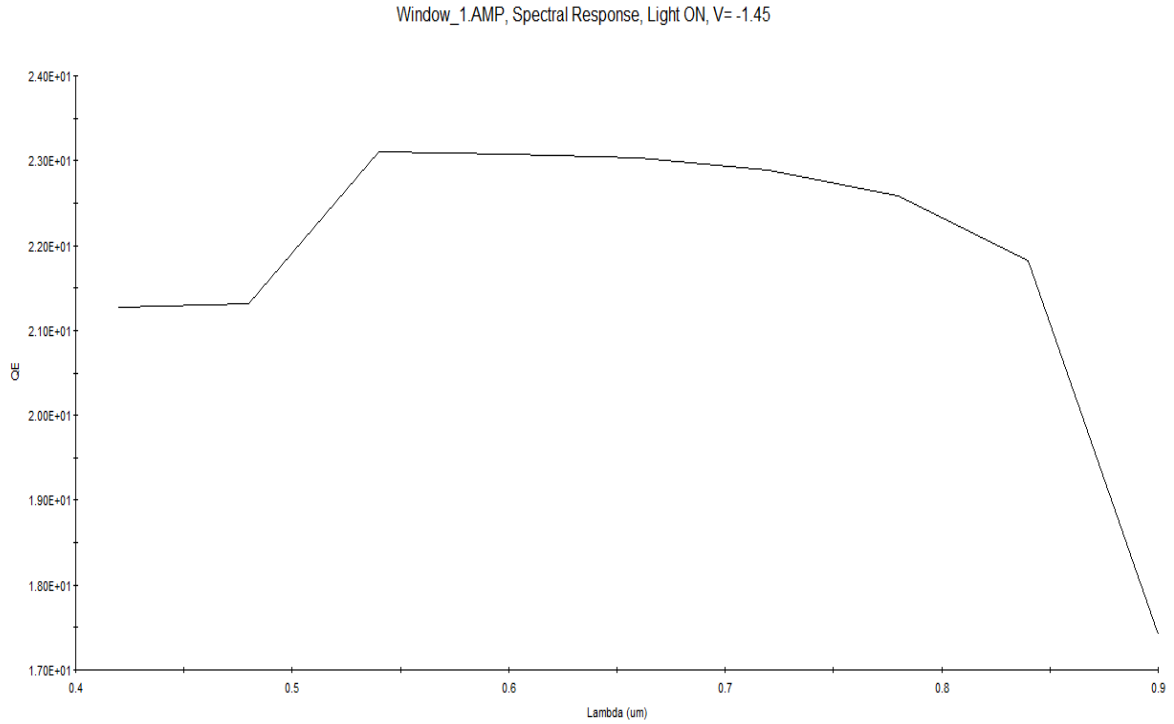

Fig. 4.10 Spectral response for $Cd_{1-x}Zn_xS/CdTe$ solar cell having window layer with x = 0.2

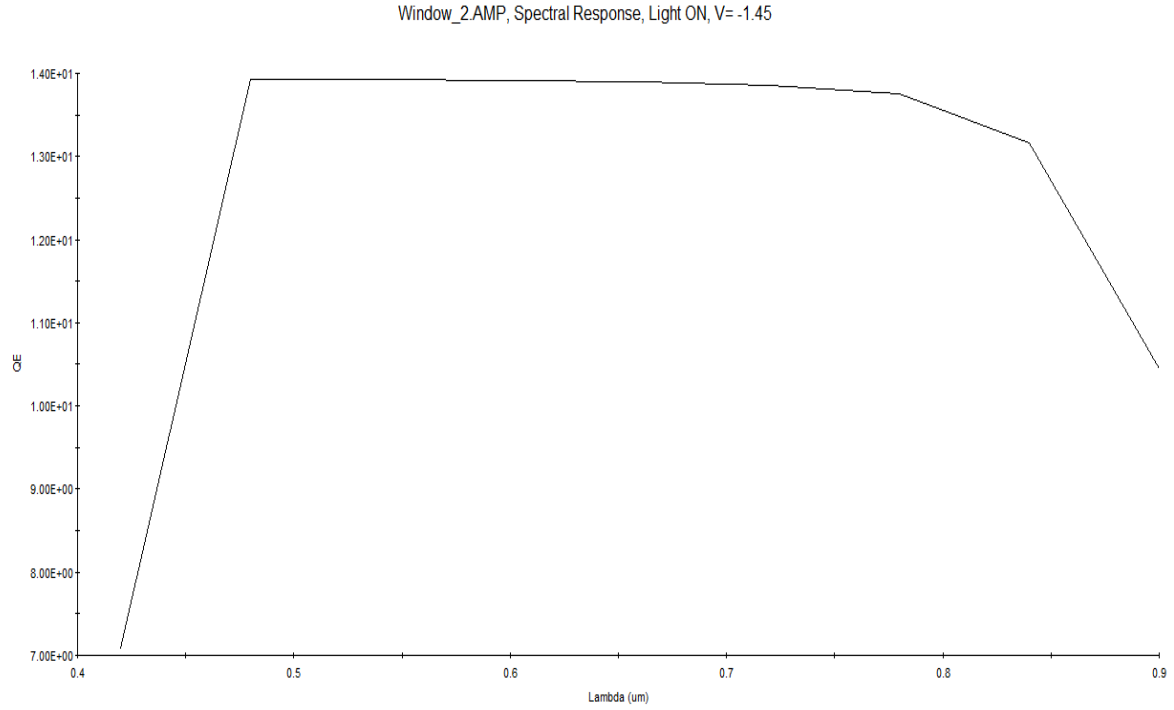

Fig. 4.11 Spectral response for $Cd_{1-x}Zn_xS/CdTe$ solar cell having window layer with x = 0.4

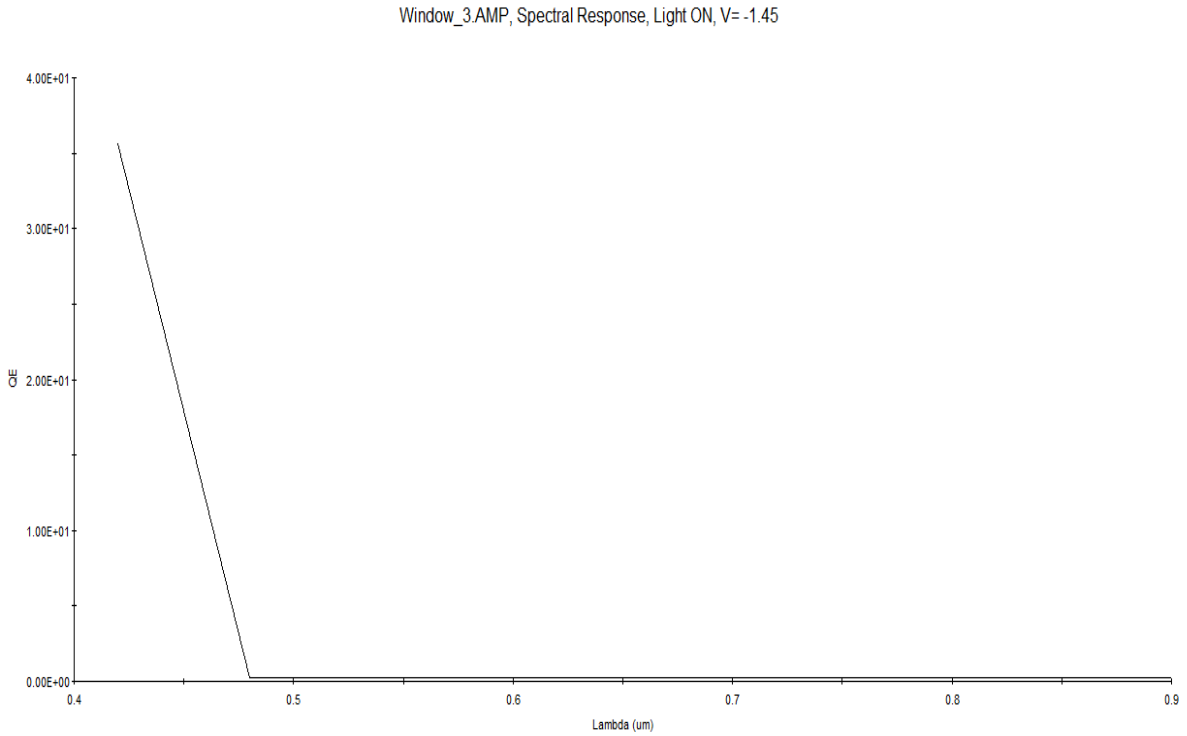

Fig. 4.12 Spectral response for $Cd_{1-x}Zn_xS/CdTe$ solar cell having window layer with x = 0.6

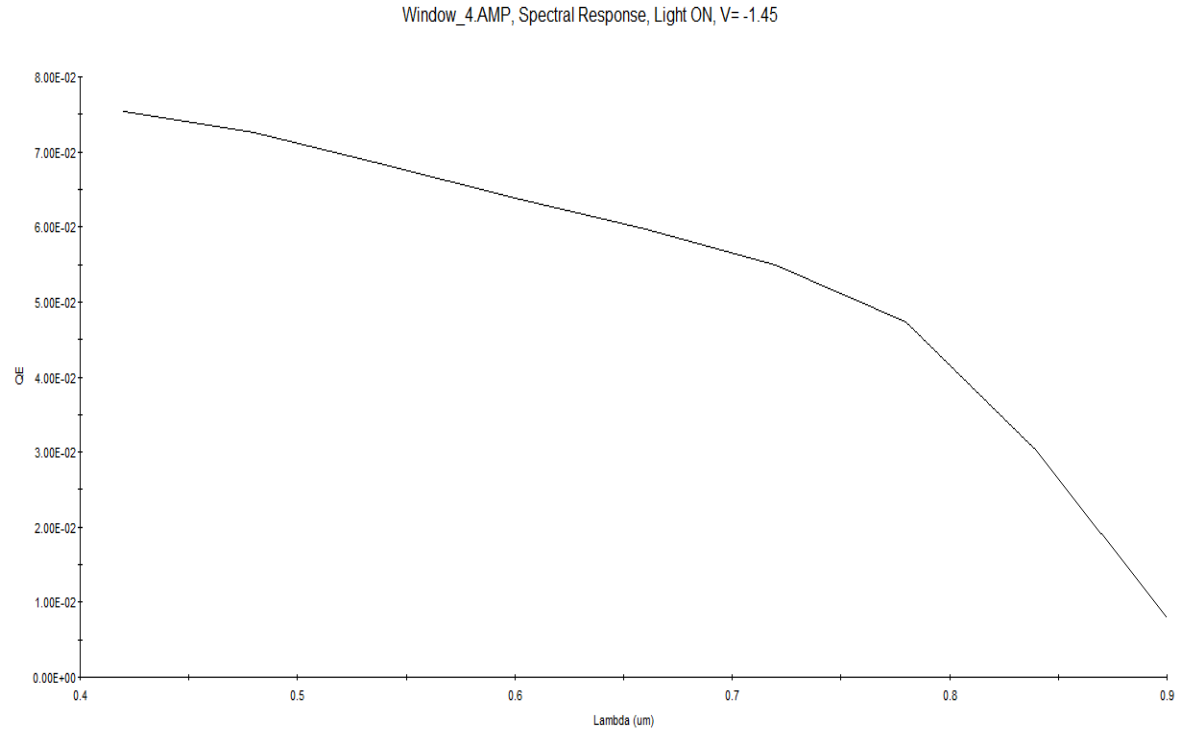

Fig. 4.13 Spectral response for $Cd_{1-x}Zn_xS/CdTe$ solar cell havingwindow layer with x = 0.8

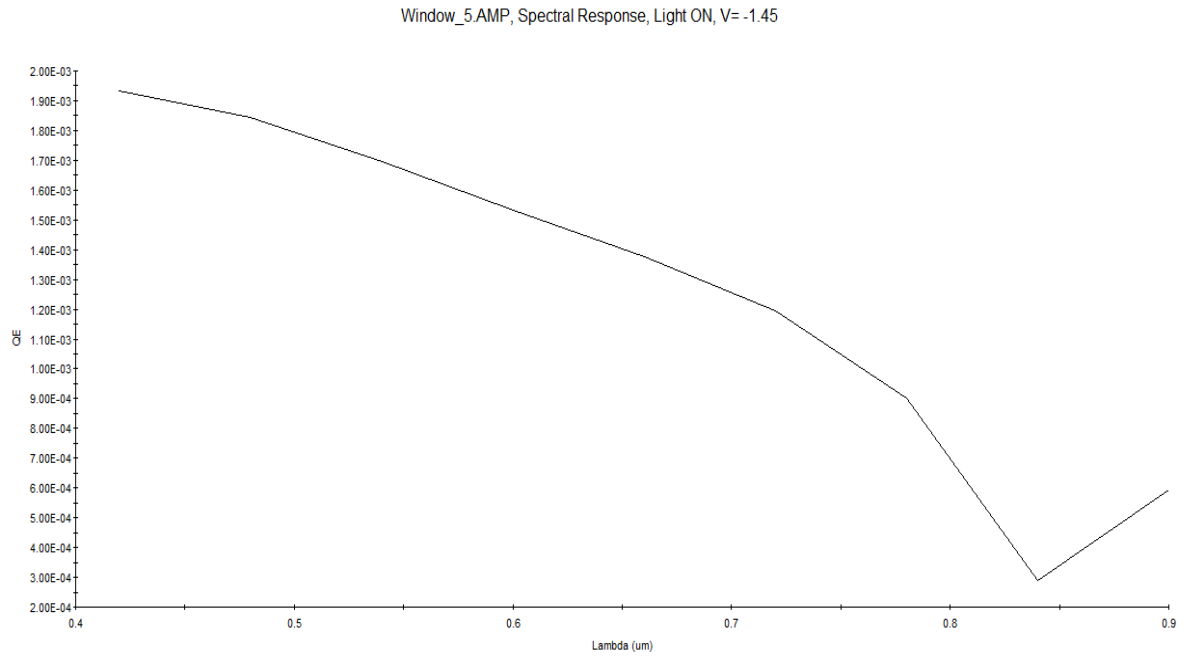

Fig. 4.14 Spectral response for $Cd_{1-x}Zn_xS$/CdTe solar cell having window layer with x = 1

Spectral response (SR) gives us an idea about the frequency specific performance of a solar cell. Ideally a flat healthy response throughout the visible spectrum of frequency is desirable. Keeping this in mind it is easily observed that for this batch of simulations SR was better for x below 0.4. From x=0. 6 the SR indicates sudden degradation and continuing that trend as x kept increasing.

4.2.3 Effect on efficiency due to variation in molar composition

Simulations were conducted for six different window layer, that six different values of x in $Cd_{1-x}Zn_xS$, keeping all other layer parameters at their default initial values. Figures 4.3-4.8 show the respective light J-V characteristics curves for these simulations. From the graph in Figure 4.15, the effect of molar composition variation on a particular output parameter, that is, the efficiency was observed. The co-dependence of energy conversion efficiency with alloy variation was analysed in this section.

From Table 4.1 and Figure 4.15 it is observed that with increase in Zn concentration in $Cd_{1-x}Zn_xS$, the efficiency tends to decrease from x=0.4 onwards. Prior to that, for a small region (from x=0 to x=0.2), the efficiency showed an upward trend, although slightly. This fact is

important as it suggests that, for a certain mixture of CdS and ZnS, the efficiency can reach higher than both of the constituent binary compound. As the efficiency is product of Voc, Jsc and FF, it will be more prudent to observe the effect of alloy variation on those unique output parameters.

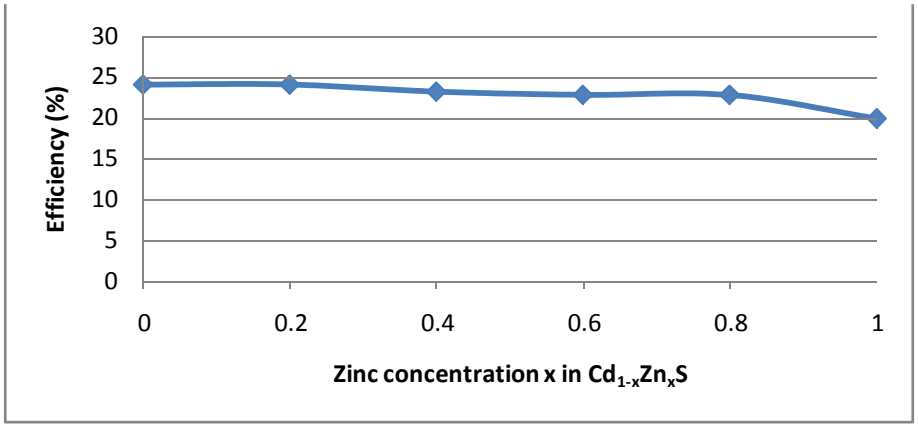

Fig. 4.15 Effect of Zn concentration x% on cell efficiency in the $Cd_{1-x}Zn_xS$/CdTe solar cell.

4.2.4 Effect on open circuit voltage due to variation in molar composition

Table 4.1 and Figure 4.16 show the effect of alloy variation on open circuit voltage (Voc). Voc for the initial design was recorded as -0.927 V. This analysis was conducted to investigate the effect of Zn in $Cd_{1-x}Zn_xS$ on open circuit voltage to give us an insight of the modified window layer performance.

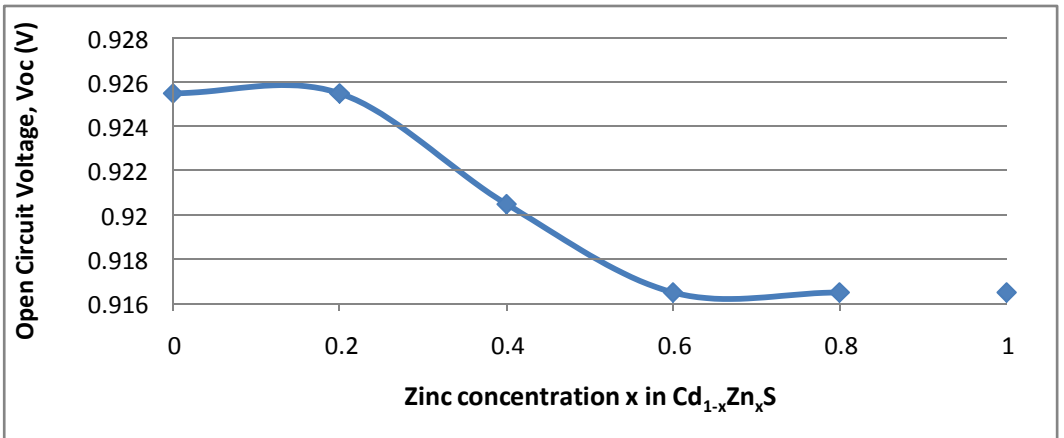

Fig. 4.16 Effect of Zn concentration x% on open circuit voltage (Voc) in the $Cd_{1-x}Zn_xS$/CdTe solar cell.

.
As it is seen from Figure 4.16, three sets of trend are observed. From x=0 to x=0.2, we observe unchanged Voc value. From x=0.2 onwards the Voc decreases until x=0.6. From x=0.6, it remains again almost unchanged. The highest Voc was observed at x=0 ~ 0.2 having a value of 0.927, exactly same as our initial design. Form this it can be deduced that, between x=0 to x=0.2 (our area of interest according to fig. 4.16), the variation in molar composition has no effect on open circuit voltage (Voc)

4.2.5 Effect on short circuit current due to variation in molar composition

In this section, analysis of the effect of alloy variation on short circuit current density (Jsc) was performed. Figure 4.17 shows the effect of Zn concentration in $Cd_{1-x}Zn_xS$ on the cell"s short circuit current density (Jsc).

Figure 4.17 shows that initially with increase in x values the Jsc increased up to x=0.6, from that point onwards Jsc took a downward dive dramatically. The highest Jsc was recorded at x=0.6 with a value of 33.105 (mA/cm^2). The initial design had a Jsc of 33.064 (mA/cm^2). It was expected as increasing x meant increasing bandgap. For a window layer increased bandgap results in more photons being let through and more carrier current, hence more Jsc.

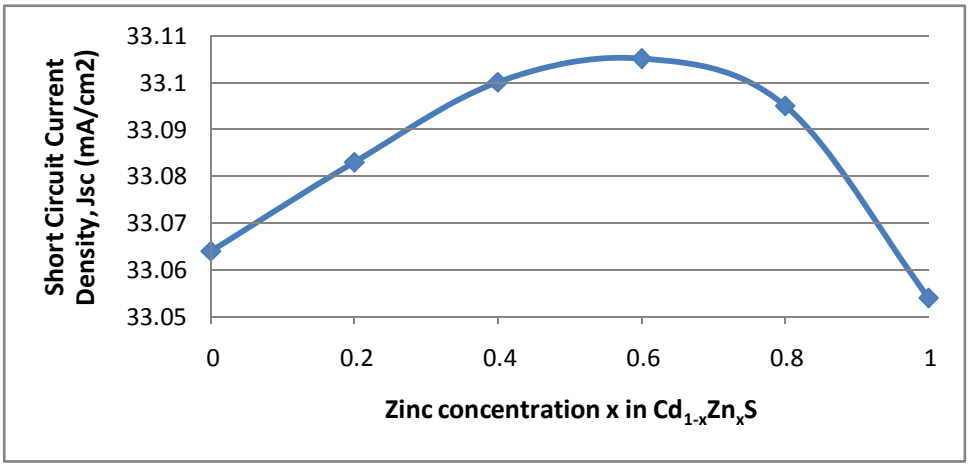

Fig. 4.17 Effect of Zn concentration x% on short circuit current density (Jsc) in $Cd_{1-x}Zn_xS$/CdTe solar cell.

4.2.6 Effect on fill factor due to variation in molar composition

Figure 4.18 shows the effect of molar composition variation on fill factor of the modified solar cell. From Figure 4.18, it is evident that FF was unchanged at 0.854 from x=0 to x=0.2. From that point onwards it decreased slowly up to x=0.8 and then dramatically after x=0.8 reaching a value of 0.711 at x=1.

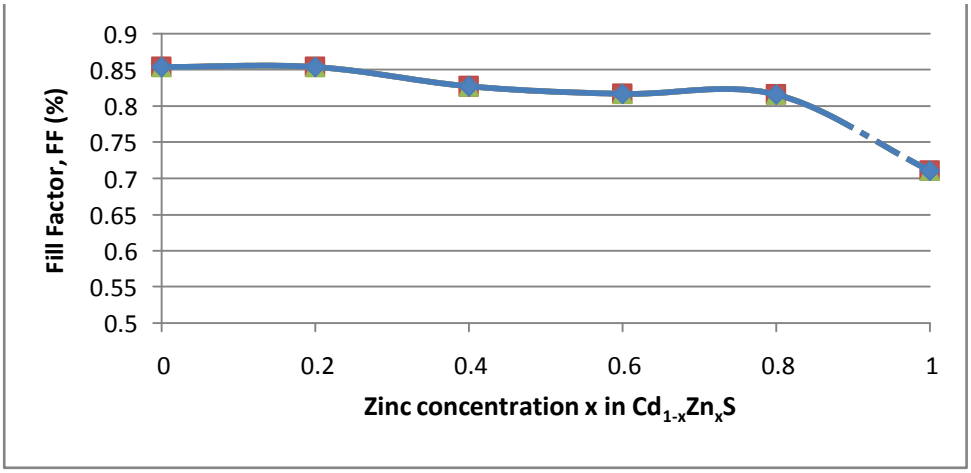

Fig. 4.18 Effect of Zn concentration x% on fill factor (FF) in the $Cd_{1-x}Zn_xS$/CdTe solar cell.

We observe, short circuit current increased with increasing Zn concentration, as bandgap was increasing letting more photons of lower wavelength through the device window, although slightly. With increase in Zn concentration, the lattice mismatch kept increasing too. This increased series resistance and ultimately lowered the fill factor (FF). Moreover, increasing Zn concentration also resulted in lower mobility and electron affinity and permittivity which further reduced FF and Voc. Decrease in Voc was less severe compared to FF.

From the analysis done above it is clear that x=0.2 gives the optimum window layer to be used in the next section. We observed this result quite evidently in the efficiency variation curve, but it is the analysis of the other output parameters that gave us better perspective and understanding. Although Jsc kept rising well beyond x=0.2 (up to x=0.6), other output parameters such as Voc and FF degraded after x=0.2. As Efficiency depends on all three output parameters (Jsc, Voc, FF) according to equation (7), it was clear why the highest efficiency occurred at x=0.2. It was result of two factors (Voc, FF) outweighing the third (Jsc).

4.3 Second modified structure with both modified window and absorber layer

After obtaining an optimum value of x in $Cd_{1-x}Zn_xS$, the second modified structure was proposed where along with the modified window layer, absorber layer was also modified by replacing CdTe with CdZnTe. Zinc mole fraction (x) in $Cd_{1-x}Zn_xTe$ was varied from 0 to 1, in steps of 0.2. The light J-V characteristics curves for x = 0-1 are given in Figures 4.19- 4.24 and spectral response in Figures 4.25- 4.30. The simulation results are summarized in table 4.2. A plot of efficiency versus Zinc mole fraction (x) in $Cd_{1-x}Zn_xTe$ is given in figure 4.31 followed by Jsc versus mole fraction, Voc versus mole fraction and FF versus mole fraction in Figures 4.32-4.34 along with lattice mismatch calculation in Table 4.3.

The results were encouraging. It was clear that with increase in Zn concentration there was moderate bandgap and lattice constant increase. Bandgap increase resulted in lower Jsc because of shifting from the optimal bandgap of 1.5 eV and going higher and absorbing less photons. The change on Jsc was significant.

On the other hand higher lattice constant meant better lattice matching which was depicted by an improved Voc and FF initially. At x=0.2 point where it seems to reach an optimum efficiency of 24.646%. Jsc was moderately high at 29.313mA/cm^2 as bandgap was still around 1.6 eV, Voc was 1.075 V and FF was 0.86. However after x=0.2, even though lattice matching kept improving along with Voc, the higher bandgaps resulted in very less Jsc.

The FF also showed declining trend but not as drastic as Jsc. The effect on Jscand to a lesser extent on FF eventually superseded the improvement on Voc and thus lowering overall efficiency drastically. The higher bandgaps were not suitable for an absorber layer which resulted in less absorption and ultimately less efficiency.

Table 4.2

Simulation Results for Different Alloy Compositions of Cadmium Zinc Telluride

X in $Cd_{1-x}Zn_xTe$	Energy Gap (eV)	Jsc (mA/ cm^2)	Voc (V)	FF	η (%)
0	1.45	33.1	0.922	0.827	22.935
0.2	1.6	29.319	1.075	0.86	24.646
0.4	1.73	27.711	1.145	0.821	23.673
0.6	1.88	16.909	1.342	0.737	15.202
0.8	2.05	13	1.506	0.684	12.406
1	2.25	9.126	1.697	0.566	7.972

4.3.1 Light J-V curves

Figure 4.19 to 4.24 illustrate the light J-V characteristics of the new solar cell design with modified absorber layer. Simulations for six different values of x (x=0, 0.2, 0.4, 0.6, 0.8 and 1) in $Cd_{1-x}Zn_xTe$ were run, which resulted in six unique light J-V curves shown below.

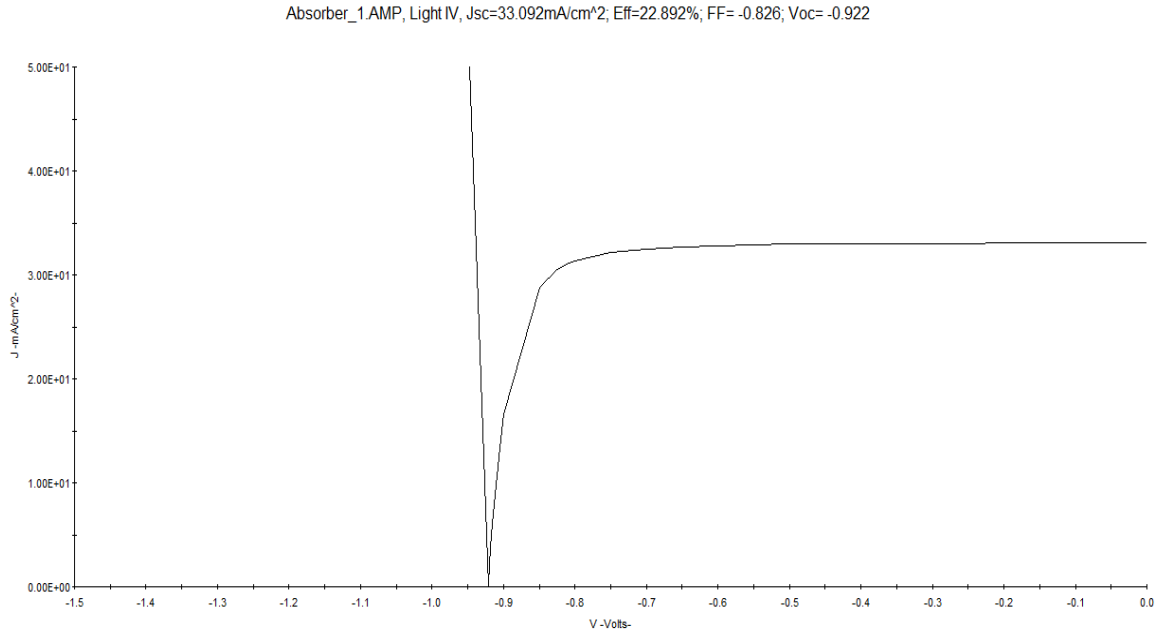

Fig. 4.19 Light J-V characteristics for $Cd_{0.8}Zn_{0.2}S/Cd_{1-x}Zn_xTe$ solar cell having absorber layer with x = 0

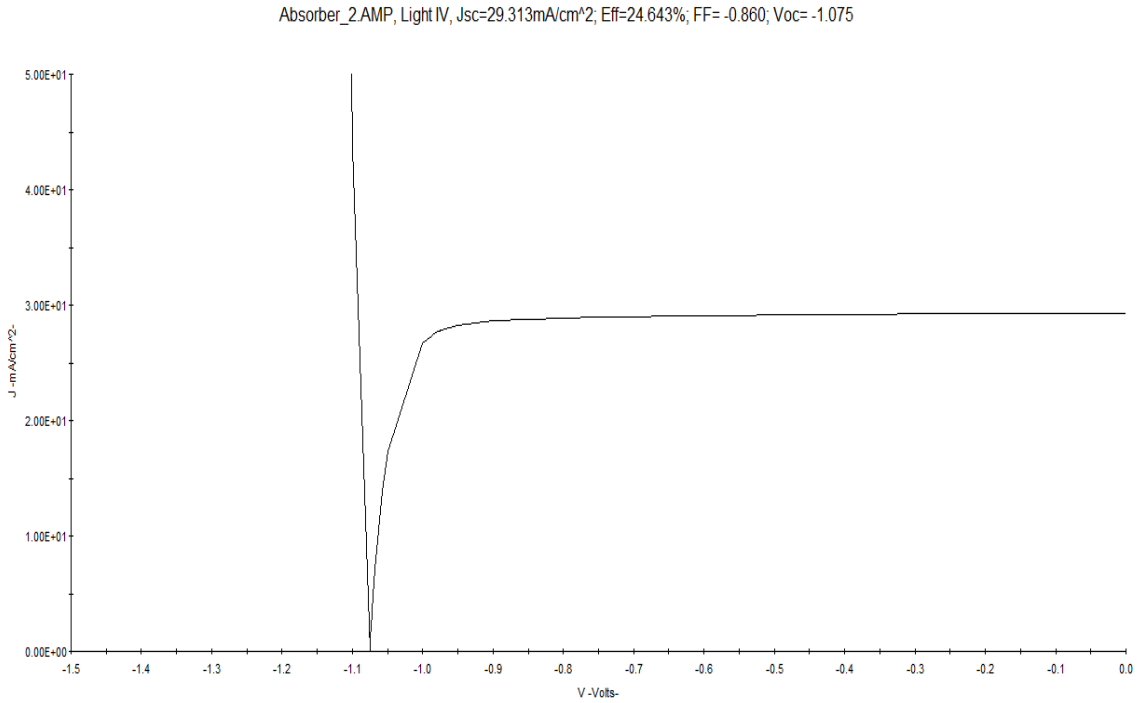

Fig. 4.20 Light J-V characteristics for $Cd_{0.8}Zn_{0.2}S/Cd_{1-x}Zn_xTe$ solar cell having absorber layer with x = 0.2

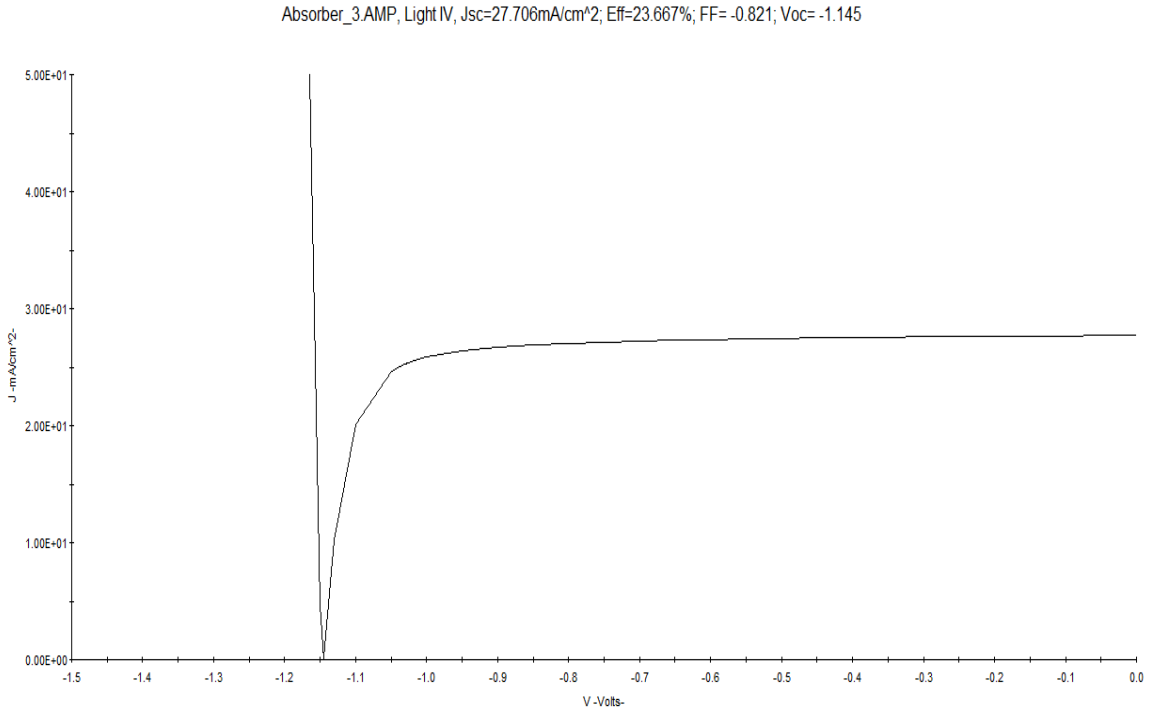

Fig. 4.21 Light J-V characteristics for $Cd_{0.8}Zn_{0.2}S/Cd_{1-x}Zn_xTe$ solar cell having absorber layer with x = 0.4

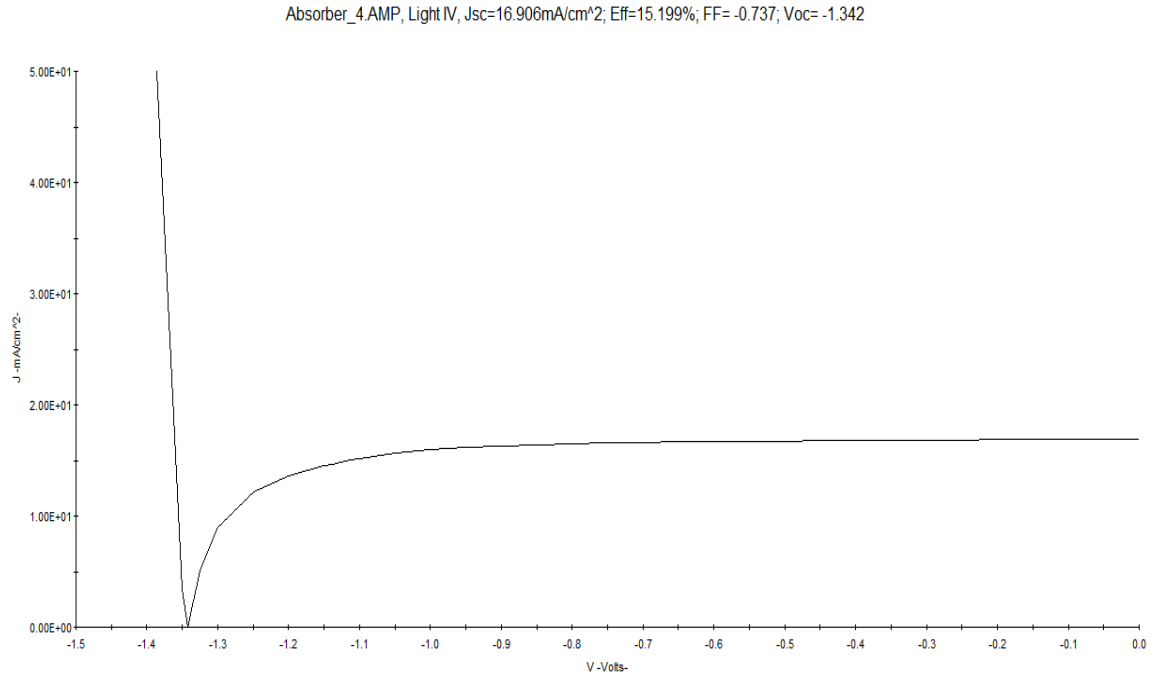

Fig. 4.22 Light J-V characteristics for $Cd_{0.8}Zn_{0.2}S/Cd_{1-x}Zn_xTe$ solar cell having absorber layer with x = 0.6

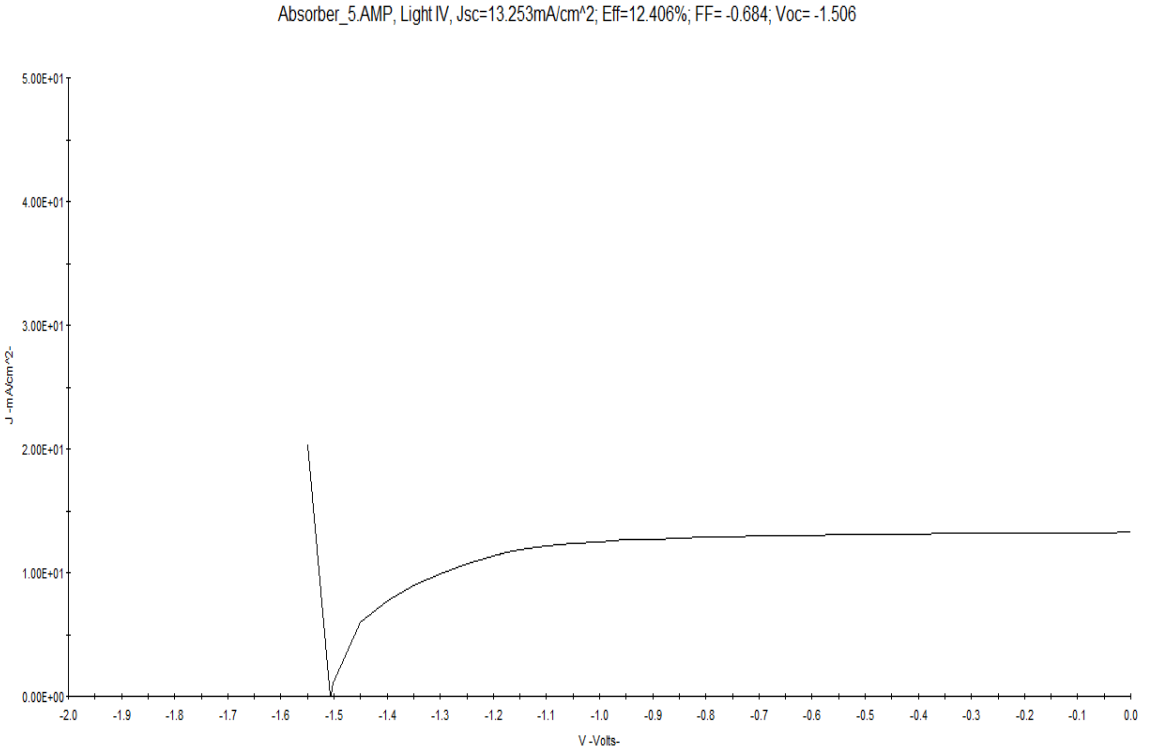

Fig. 4.23 Light J-V characteristics for $Cd_{0.8}Zn_{0.2}S/Cd_{1-x}Zn_xTe$ solar cell having absorber layer with x = 0.8

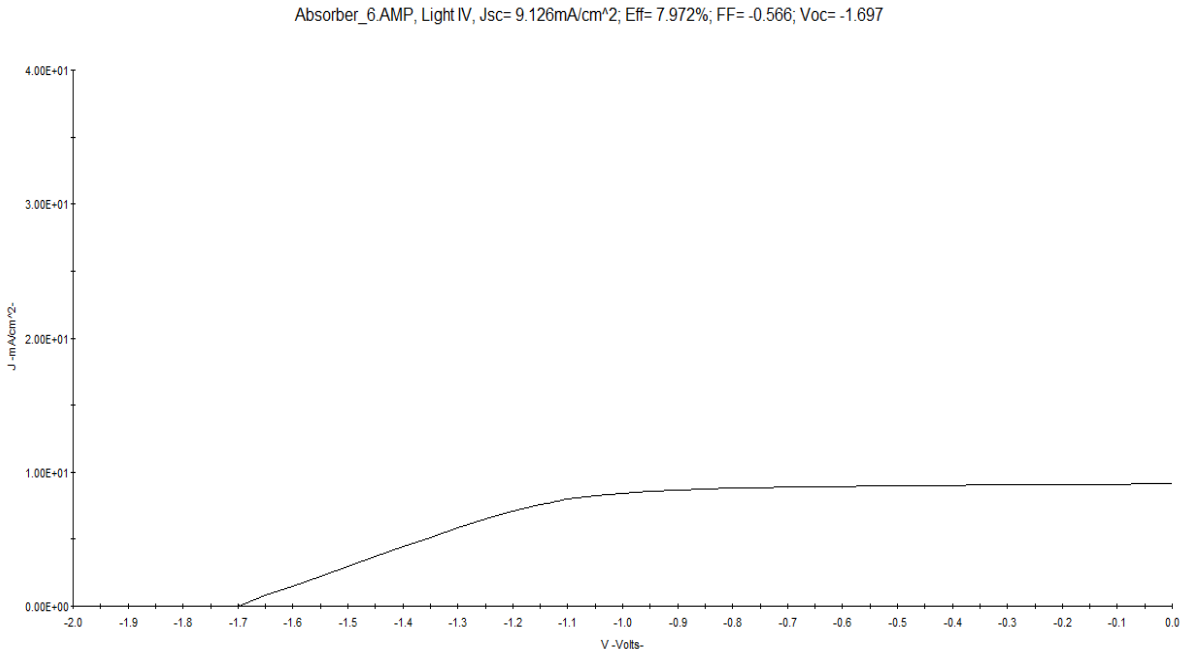

Fig. 4.24 Light J-V characteristics for $Cd_{0.8}Zn_{0.2}S/Cd_{1-x}Zn_xTe$ solar cell having absorber layer with x = 1

4.3.2 Spectral Responses

To better understand the frequency response of the modified solar cell, spectral responses (SR) for different simulations were shown in Figure 4.25 to 4.30.

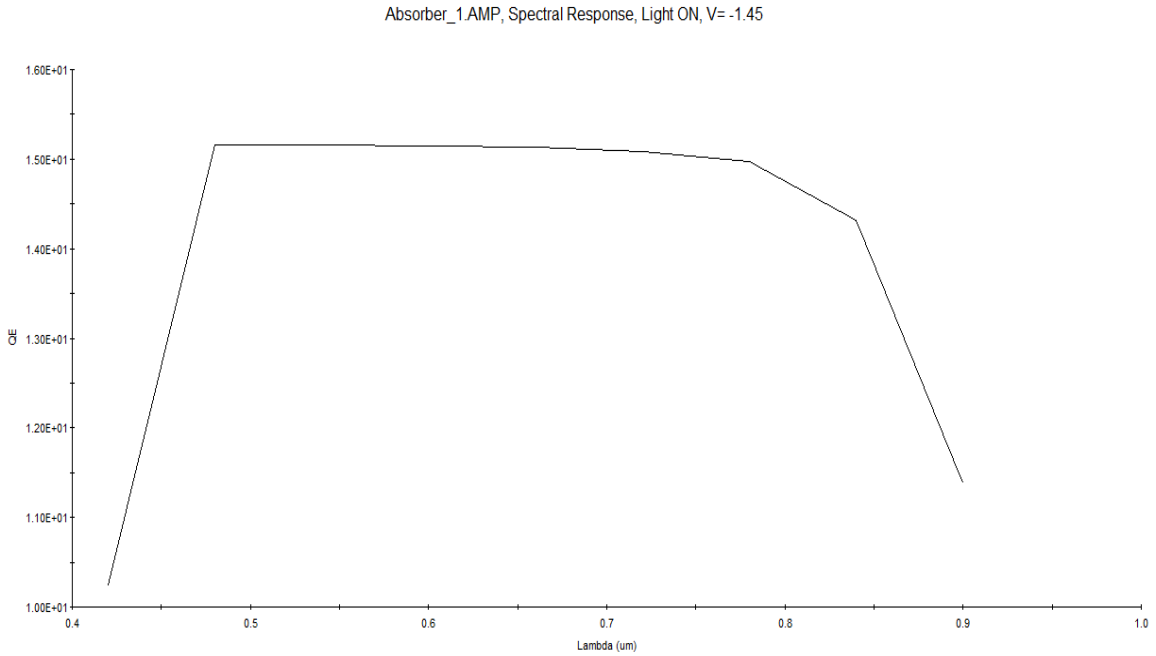

Fig. 4.25 Spectral response for $Cd_{0.8}Zn_{0.2}S/Cd_{1-x}Zn_xTe$ solar cell having absorber layer with x = 0

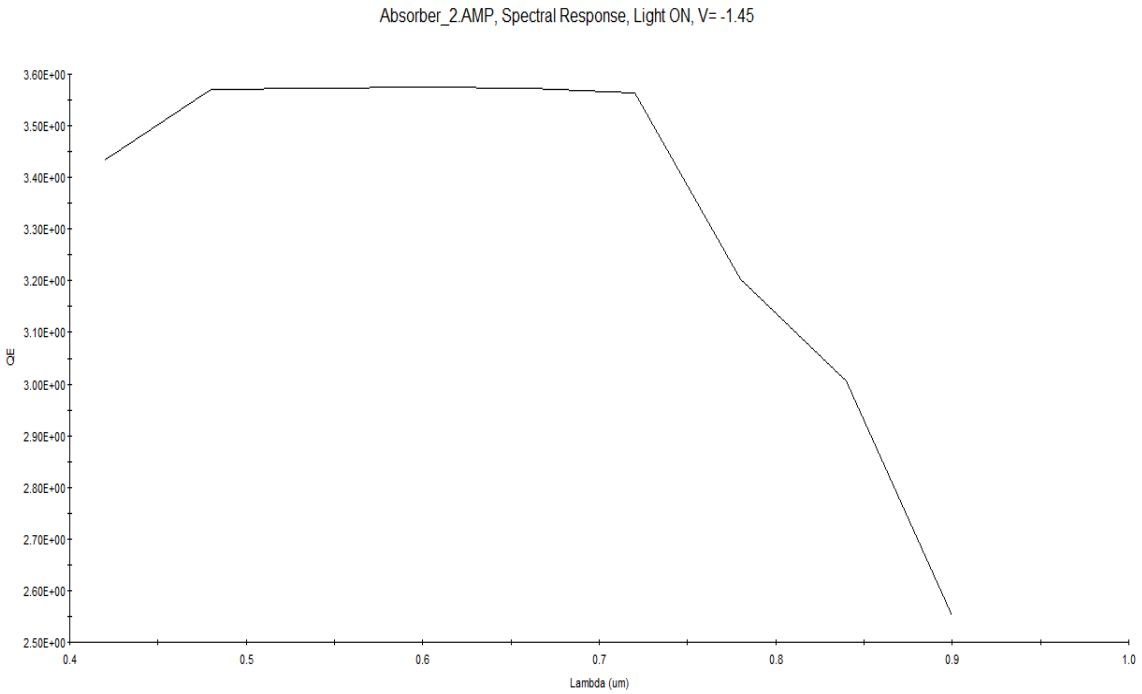

Fig. 4.26 Spectral response for $Cd_{0.8}Zn_{0.2}S/Cd_{1-x}Zn_xTe$ solar cell having absorber layer with x = 0.2

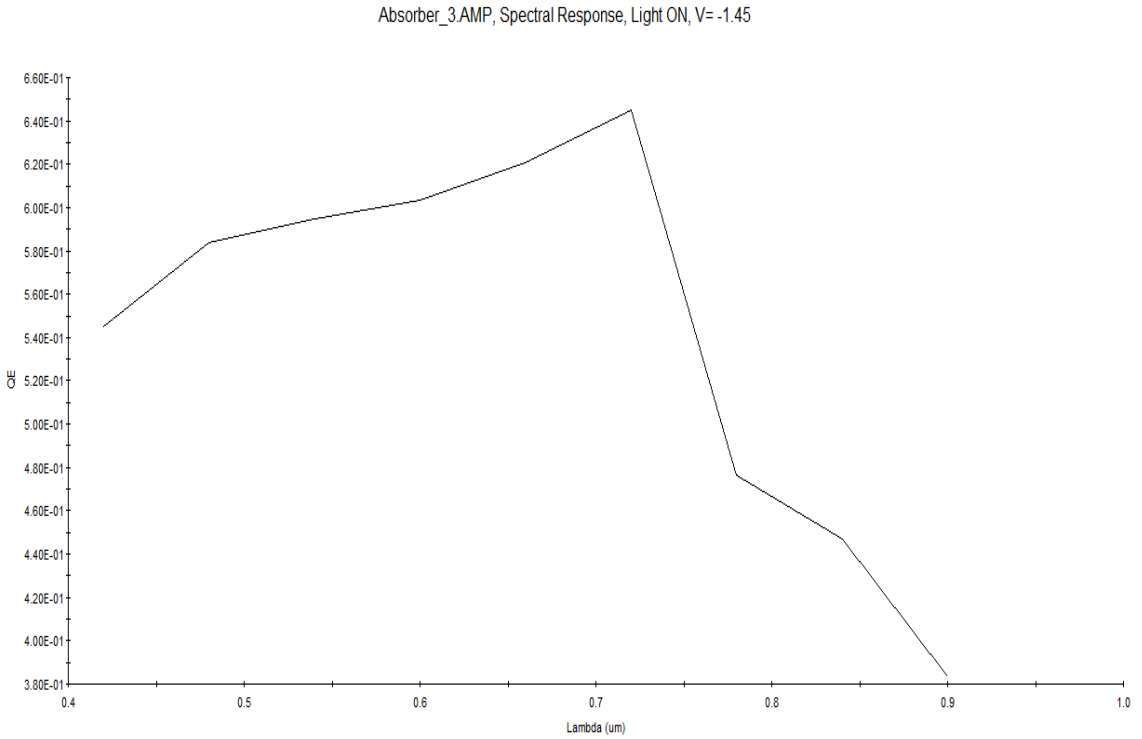

Fig. 4.27 Spectral response for $Cd_{0.8}Zn_{0.2}S/Cd_{1-x}Zn_xTe$ solar cell having absorber layer with x = 0.4

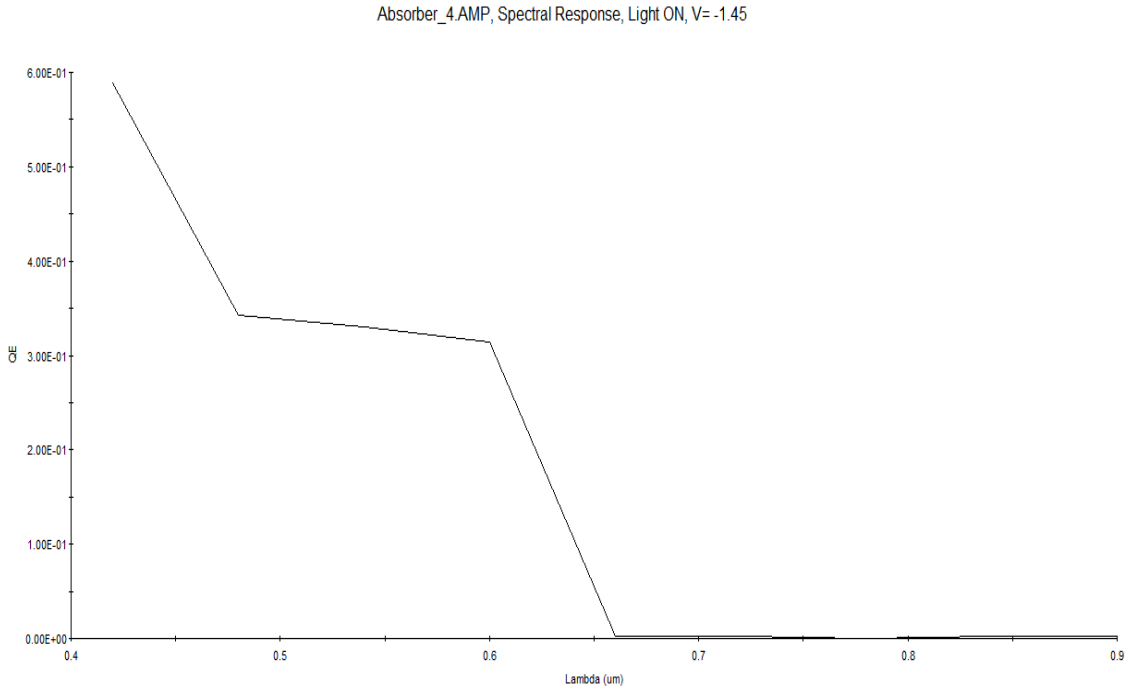

Fig. 4.28 Spectral response for $Cd_{0.8}Zn_{0.2}S/Cd_{1-x}Zn_xTe$ solar cell having absorber layer with x = 0.6

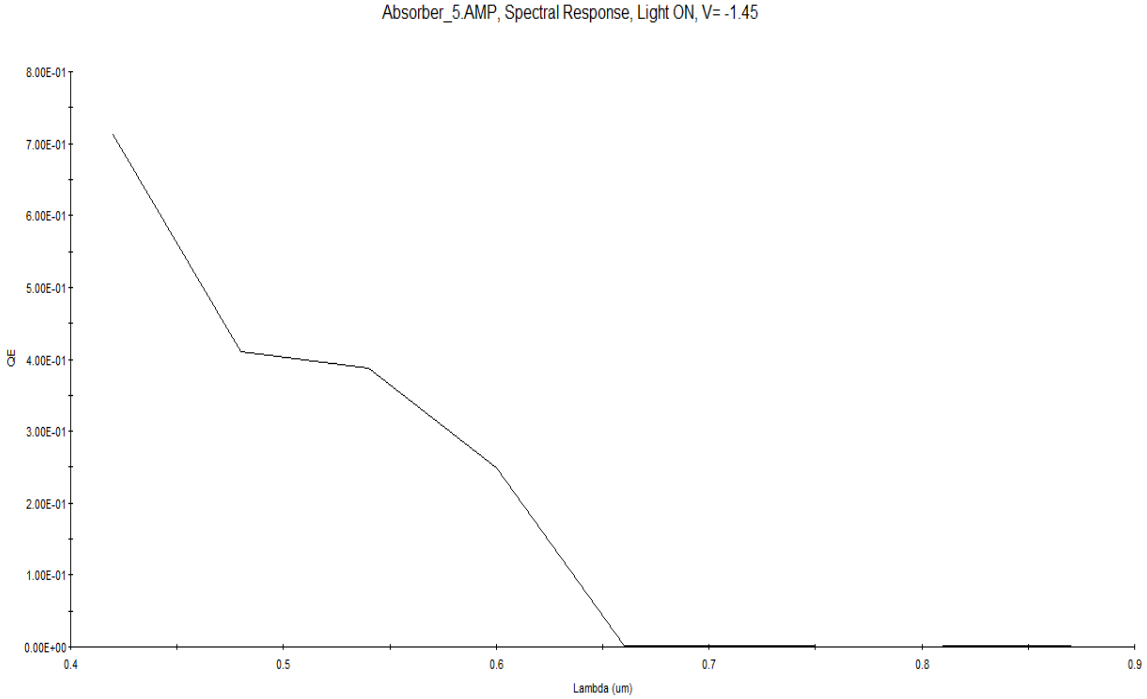

Fig. 4.29 Spectral response for $Cd_{0.8}Zn_{0.2}S/Cd_{1-x}Zn_xTe$ solar cell having absorber layer with x = 0.8

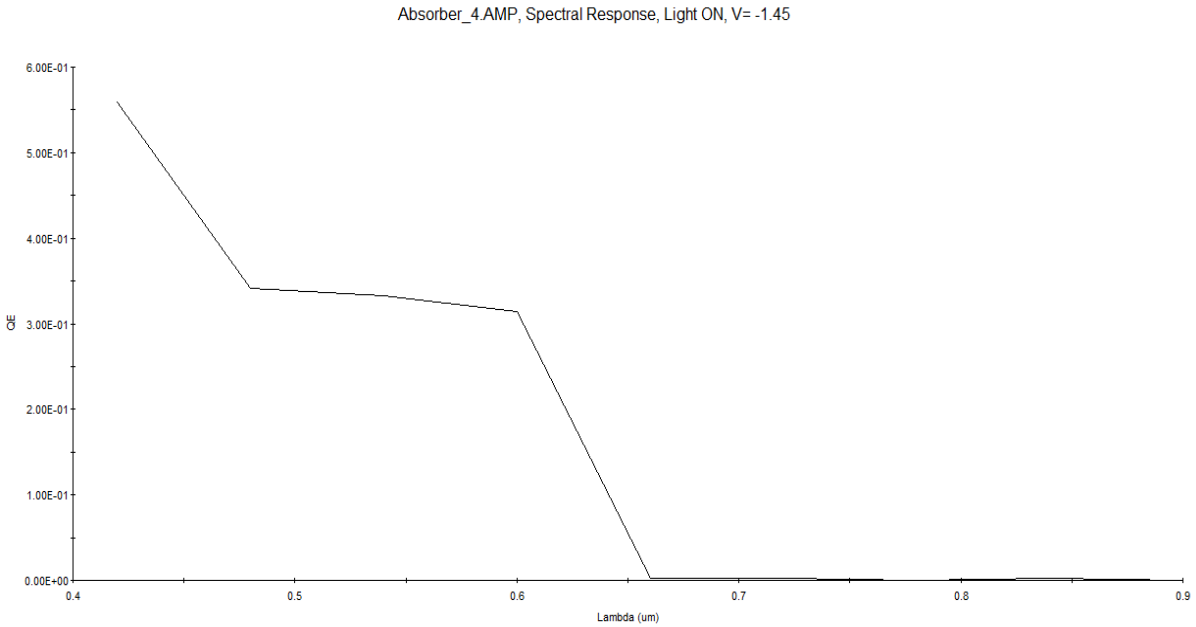

Fig. 4.30 Spectral response for $Cd_{0.8}Zn_{0.2}S/Cd_{1-x}Zn_xTe$ solar cell having absorber layer with x = 1

The SR of this batch of simulations shows gradual decrease in QE for x value. Along with decreased QE, the cut off frequency also decreases with increase in x value indicating a poor spectral response as x increases. The cut off frequency was around 0.9 µm for x=0 and after gradual decrease, it ended up at around 0.6 at x=1.

4.3.3 Effect on efficiency due to variation in molar composition

Figure 4.31 illustrates the analysis of efficiency dependence on molar variation for the modified cell design having $Cd_{1-x}Zn_xTe$ as absorber. This analysis will provide us with a better understanding of the convoluted effect molar composition variation has on different output parameters.

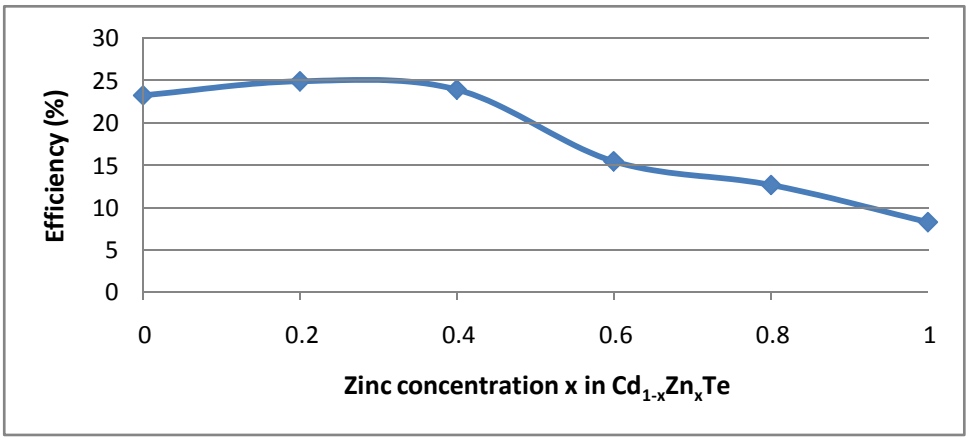

Fig. 4.31 Effect of Zn concentration x% on Efficiency in the $Cd_{0.8}Zn_{0.2}S/Cd_{1-x}Zn_xTe$ solar cell

The graph in figure 4.31 shows that higher efficiencies are obtained as the Aluminium mole fraction is increased in $Cd_{1-x}Zn_xTe$ from x=0 to x=0.2. The top layer ($Cd_{1-x}Zn_xS$ layer) acts like a window layer [29] in the heterojunction solar cell, as mentioned in section 2.2.

It is an established fact that the optical absorption in the base (absorber) layer increases with higher bandgap of the window layer material [8, 26]. Higher optical absorption leads to higher output current and, as a result, higher efficiency. But it is observed that from x=0.2 to x=0.4 there is slight decline in efficiency and beyond that the decline is quite dramatic. Investigation in to the constituent output parameters (Voc, Jsc and FF) of the efficiency equation might provide with a better explanation as to why this happens.

4.3.4 Effect on open circuit voltage due to variation in molar composition

Figure 4.32 shows the effect of varying molar composition on open circuit voltage of the modified solar cell. As mentioned earlier simulations were run for different x values (x= 0 to 1 with step of 0.2) in $Cd_{1-x}Zn_xTe$, which is the modified absorber layer in the solar cell investigated in this chapter.

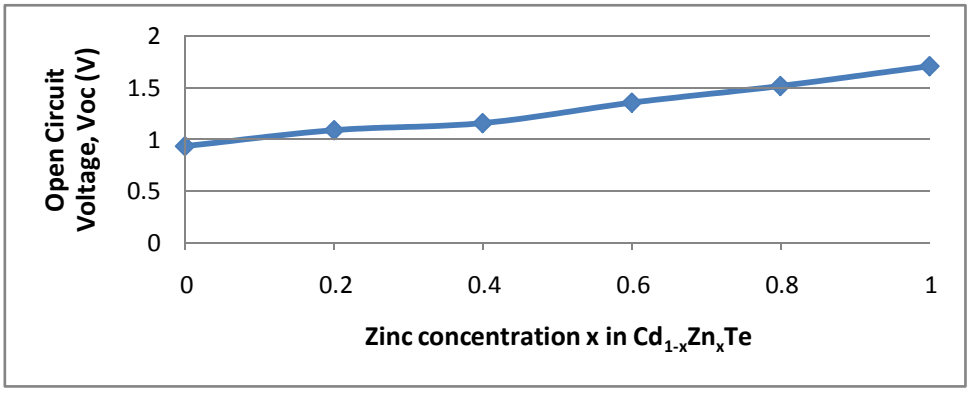

Fig. 4.32 Effect of Zn concentration x% on open circuit voltage (Voc) in the $Cd_{0.8}Zn_{0.2}S/Cd_{1-x}Zn_xTe$ solar cell

Figure 4.32 clearly suggest that with an increase in Zn concentration in $Cd_{1-x}Zn_xTe$ the Voc of the modified solar cell increases. The increase is almost linear with a slight dip in x=0.4 value.

The graph in Figure 4.32 also shows that the highest level of efficiency is obtained when Zinc mole fraction in $Cd_{1-x}Zn_xTe$ near 1. So, this individual investigation suggests, the value of x in $Cd_{1-x}Zn_xTe$ should be kept near 1 for optimization.

4.3.5 Effect on short circuit current due to variation in molar composition

Zinc mole fraction (x) in $Cd_{1-x}Zn_xTe$ was varied from 0 to 1, in steps of 0.2 and was plotted against respective short circuit current density Jsc. The simulation outcomes are shown in Figure 4.33.This analysis was done to understand the effect of alloy variation on Jsc of this particular solar cell design.

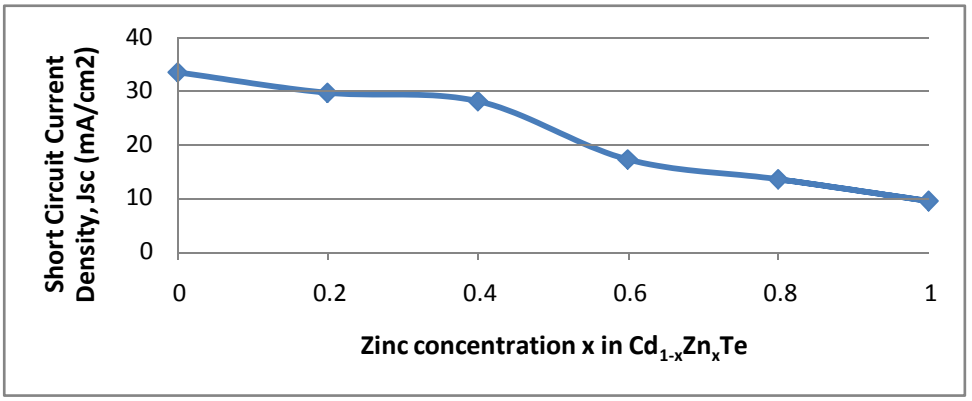

Fig. 4.33 Effect of Zn concentration x% on short circuit current density (Jsc) in$Cd_{0.8}Zn_{0.2}S/Cd_{1-x}Zn_xTe$ cell

From the figure it seems that short circuit current decrease with increase in Zn concentration in $Cd_{1-x}Zn_xTe$ in the solar cell. The decline is less from x=0 to x=0.4 but after that the decline is more severe. This investigation suggests that x value should be kept as low as possible, quite the opposite result from the last observation.

4.3.6 Effect on fill factor due to variation in molar composition

Figure 4.34 correlates the fill factor (FF) with the variation in the molar composition. As usual, simulations were run for x=0 to1 with a step of 0.2.

The result in this section is quite interesting. Generally with increase in Zn concentration the FF tends to decrease with the exception at x=0.2 where the FF increased from x=0 before going in a declining trend. It suggests that x=0.2 can be chosen as an optimum value for a better FF for this solar cell.

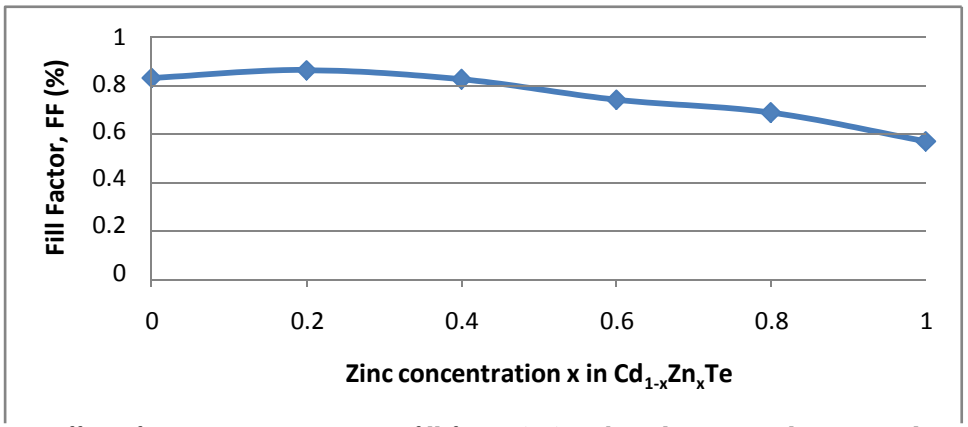

Fig. 4.34 Effect of Zn concentration x% on fill factor (FF) in the $Cd_{0.8}Zn_{0.2}S/Cd_{1-x}Zn_xTe$ solar cell

4.3.7 Lattice mismatch

Lattice mismatches in different alloy compositions for two batches of simulations were also calculated using linear equation stated earlier. The findings are listed in Table 4.3. The lattice mismatching of modified $Cd_{0.8}Zn_{0.2}S$ /$Cd_{0.8}Zn_{0.2}Te$ was found to be 10.16%, which resembles the original CdS/CdTe lattice mismatch but this structure yielded better Jsc and Voc that ultimately resulted in a high efficiency solar cell.

Table 4.3

Calculated lattice mismatch (%) for various simulations

Zinc x%	$Cd_{1-x}Zn_xS$ / CdTe	$Cd_{0.8}Zn_{0.2}S/Cd_{1-x}Zn_xTe$
0	10	11.2
0.2	11.2	10.16
0.4	12.6	9.2
0.6	13.8	8.06
0.8	15.1	6.93

The effect of varying Zn concentration on different output parameters of a $Cd_{0.8}Zn_{0.2}S$ /$Cd_{1-x}Zn_xTe$ solar cell was illustrated in Figure 4.31 to 4.34. The trend shown by Jsc (decreasing with increasing x%) and Voc (increasing with increasing x%) is quite straight forward. The FF however, showed interesting results. FF initially increased for x=0.2 but later showed declining trend before taking a drastic fall near x=0.6. So near x=0.2, the improved FF along with high Voc and moderate Jsc can be utilized for an optimum efficiency for this particular solar cell structure. Further study is warranted to investigate the mechanism taking place in this area of interest where Voc seems to improve just before degrading for a $Cd_{1-x}Zn_xTe$ absorber layer. So in this chapter an optimum solar cell of $Cd_{0.8}Zn_{0.2}S/Cd_{0.8}Zn_{0.2}Te$ instead of initial CdS/CdTe is proposed that provides a better bandgap for the window layer and reduces lattice mismatch between modified window and absorber layer.

4.4 Optimization of Alloy Composition

From the previous two sections it was clear that optimum value of x is 0.2 for both window and absorber layer. So initial design of TCO/ZnO/CdS/CdTe/Cu_2Te/Ni was first modified to a structure of TCO/ZnO/$Cd_{0.8}Zn_{0.2}S$/CdTe/Cu_2Te/Ni. Then in the second modification, a new structure was formed, namely TCO/ZnO/$Cd_{0.8}Zn_{0.2}S/Cd_{0.8}Zn_{0.2}Te$/$Cu_2Te$/Ni. This last structure serves as the optimum structure in terms of optimized molar composition in both ternary window and absorber layer.

4.4.1 Effect of varying window thickness on the optimized structure

Table 4.4 and Figure 4.35 illustrate the effect of window thickness on the overall cell performance in terms of efficiency.

As it is seen from the figure and table, efficiency decreases with increasing window layer thickness. This is an expected outcome, because the window layer actually acts like a window [29]. Short-circuit current and optical absorption capability of the device is improved with a thinner window layer [34], which is supported by table 4.4. So, minimization of top layer

thickness, and maximization of base layer thickness will be an important step towards optimization.

Table 4.4

Simulation Results for Varying Window Layer Thickness

Window Layer Thickness (μm)	V_{oc} (V)	J_{sc} (mA/cm^2)	FF	Efficiency (η%)
0.1	1.075	29.276	0.859	24.578
0.2	1.075	29.194	0.851	24.284
0.3	1.074	29.001	0.841	23.817
0.4	1.074	28.596	0.834	23.289
0.5	1.073	28.045	0.833	22.79
0.6	1.073	27.468	0.835	22.362
0.7	1.072	26.942	0.838	22.015
0.8	1.072	26.5	0.842	21.741
0.9	1.072	26.147	0.845	21.53
1	1.072	25.871	0.848	21.369

Figure 4.35clearly suggests a decline in performance with increase in window thickness in the modified solar cell. So, for an optimum performance the thickness of a window layer should be kept at minimum in accordance with fabrication and cost restriction. A 100 nm window layer solar cell produces around 25% efficiency whereas a 900 nm only produces 21.5%.

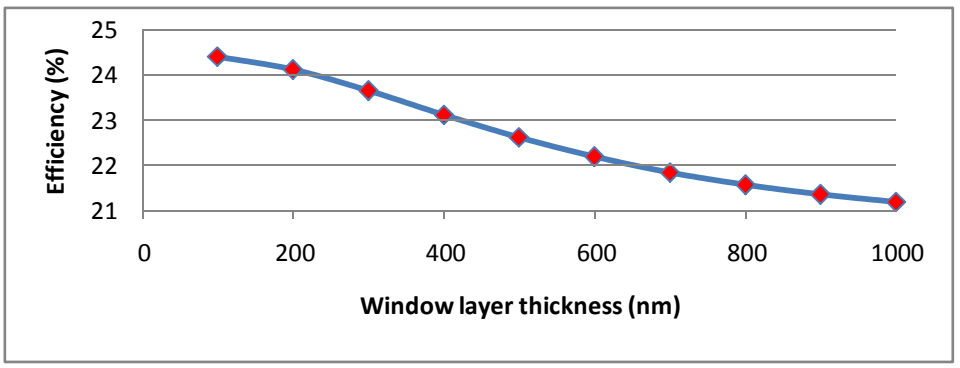

Fig 4.35 Efficiency variation with window layer thickness

4.4.2 Effect of varying absorber thickness on the optimized structure

The effect of absorber layer thickness on cell efficiency is analysed through Table 4.5 and Figure 4.36. This investigation aims to find an optimum absorber thickness and understand the dynamics of thickness versus efficiency relationship.

Table 4.5

Simulation Results for Varying Absorber Layer Thickness

Absorber Thickness (μm)	**V_{oc} (V)**	**J_{sc} (mA/cm^2)**	**FF**	**Efficiency (η%)**
1	1.075	29.319	0.86	24.643
2	1.059	28.6766	0.84	23.184
3	1.053	27.741	0.833	22.114
4	1.051	27.052	0.831	21.479
5	1.05	26.662	0.831	21.12
6	1.049	26.362	0.832	20.915
7	1.049	26.206	0.832	20.796
8	1.049	26.112	0.832	20.726
9	1.049	26.061	0.833	20.688
10	1.049	26.026	0.833	20.661

Now, we have conducted a number of simulations with varying base layer thickness values, in order to give us a good number of options for the efficiency and cost trade-off. Table 4.5 lists the simulation outcomes. A graph of efficiency versus absorber layer thickness of the modified design is shown in figure 4.36.

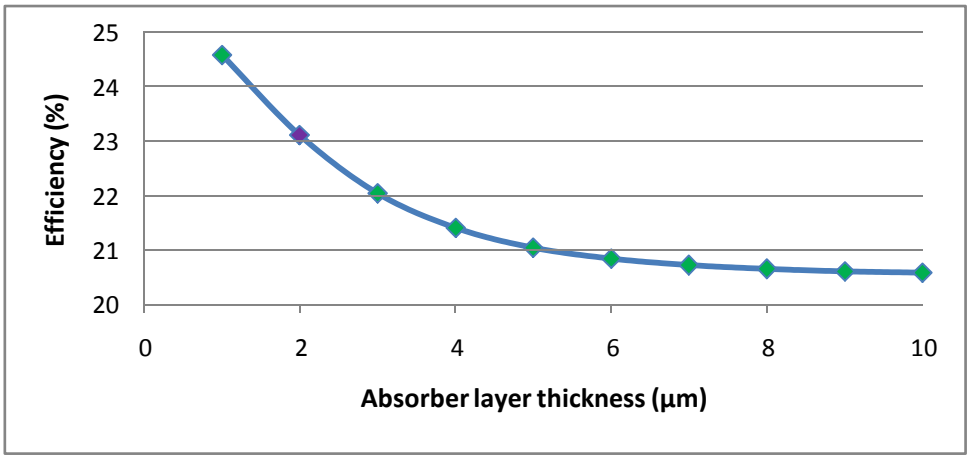

Fig 4.36 Efficiency variation with absorber layer thickness

The figure 4.36along with table 4.5 suggests an inverse relation between absorber thickness and efficiency. Higher efficiencies are obtained with absorber of lower thickness. From 1 µm to 4 µm thickness the decrease in efficiency is almost linear. After 4 µm to 10 µm thickness the efficiency seems to be unaffected by absorber thickness. This finding can give us some interesting and cost effective options.

4.4.3 Effect of operating temperature on the optimized structure

The performance of optimized structure $Cd_{0.8}Zn_{0.2}S$ /$Cd_{0.8}Zn_{0.2}Te$ also showed good temperature stability over a range of higher temperature. Figure 4.37 illustrates effect of temperature on modified solar cell efficiency. T_c (temperature coefficient) was found to be 0.05 %/ C^0.

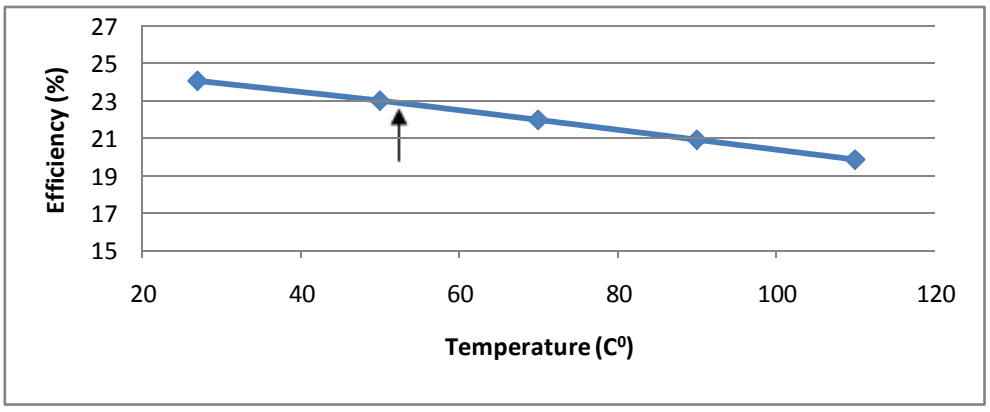

Fig 4.37 Efficiency variation with temperature

Remarks

First batch of simulations involving modified window layer of $Cd_{1-x}Zn_xS$ yielded maximum efficiency of 23.815% for x=0.2 with Jsc=33.083 mA/cm^2, Voc=0.927 V and FF=0.854. A related work with $Cd_{1-x}Zn_xS$/CdTe solar cell was published by Sharafat et. al. where it reported a maximum efficiency of 19.34% for x=0.05 with Jsc=30.43 mA/cm^2, Voc=0.92 V and FF=0.759 [15].

Second batch of simulations involving modified absorber layer of $Cd_{1-x}Zn_xTe$ combined with an optimal modified window layer of $Cd_{0.8}Zn_{0.2}S$ yielded maximum efficiency of 24.646% for x=0.2 with Jsc=29.319 mA/cm^2, Voc=1.075 V and FF=0.86. Imamjai et. al. published a a work with CdS/ $Cd_{1-x}Zn_xTe$ cell structure, where, for x=0.2, the reported efficiency was 24% with Jsc=30 mA/cm^2, Voc=1.1 V and FF=0.8 [37]. This solar cell was also a lot thicker than the proposed cell in this thesis with TCO thickness of 500 nm, Window (CdS) thickness of 100 nm and absorber ($Cd_{1-x}Zn_xTe$) thickness of 4 µm. Clearly the proposed solar cell in this thesis is lot thinner (TCO=100 nm, window=50 nm, absorber= 1 µm) with superior efficiency.

The significant contribution made in this chapter is the design of a modified thin film solar cell with started with the initial cell structure and materials. In this chapter, dependence of energy conversion efficiency on alloy composition has been investigated in details for the $Cd_{1-x}Zn_xS$/ $Cd_{1-x}Zn_xTe$ heterojunction solar cell. Effect of change in alloy composition on efficiency, Jsc, Voc and FF has been analysed separately for the device. This analysis will be helpful in selecting materials with optimum combination of bandgaps for fabricating heterojunction solar cells. The results found in this chapter can provide a better insight into the way of alloy composition optimization in heterojunction and multijunction solar cells fabricated from ternary and quaternary alloys for achieving the highest possible efficiency.

Chapter 5- Summary

In this research, A small range of Zn x% in absorber (around x = 0.2) appeared where the proposed two fold treatment eventually yielded a better efficiency of 24.643% before declining. The lattice mismatching of modified $Cd_{0.8}Zn_{0.2}S$ /$Cd_{0.8}Zn_{0.2}Te$ was found to be 10.16%, which resembles the original CdS/CdTe lattice mismatch but this structure yielded better Jsc and Voc that ultimately resulted in a high efficiency solar cell. However after x=0.2, even though lattice matching kept improving along with Voc, the higher bandgaps resulted in very less Jsc. The FF also showed declining trend but not as drastic as Jsc. The effect on Jsc and to a lesser extent on FF eventually superseded the improvement on Voc and thus lowering overall efficiency drastically. The higher bandgaps were not suitable for an absorber layer which resulted in less absorption and ultimately less efficiency.

5.1 Overview of the Work

In chapter 1, an overview of the research background, outline and novelty was presented. This chapter was a gist of the thesis and research that went under in the course of it.

In chapter 2, the basic operational principles of solar cells, along with the basics of heterojunction solar cells were discussed. The application of II-VI compounds in solar cells, with an investigation into the high-cost issue of II-VI solar cells, which is the limiting factor for the mass fabrication of these solar cells were also discussed. CdTe solar cell was discussed and some major drawbacks of the CdTe solar cell were presented along with its ever increasing popularity. This served as a motivation for the thesis. A brief outline was given of this research with a discussion of the novelty in proposed device with appropriate references.

In chapter 3, the methodology of the research was described. An initial design of a CdS/CdTe heterojunction solar cell was introduced which served as the starting point of the simulation. Then two modified structure were proposed and modelled. First modification was to the window layer and second modification was to the absorber layer in conjunction with the best

window layer obtained from the first modification. Later, the final modified structure was subjected to a thorough investigation that was aimed to analyse the co dependence of cell performance to the layer thicknesses of the core layers and operating temperature.

In chapter 4, results and discussion was presented where a detailed analysis was performed for modified design in the solar cell. The modified window layer was analysed for different molar composition profiles for achieving high efficiency. A separate investigation was performed to find the change in a particular output parameter (efficiency, Voc, Jsc, FF) due to molar variation in window layer of the cell with analysis of the outcomes with proper explanation of the underlying physics. Investigation was also done to find the change in output characteristics of the device with varying alloy composition in the absorber layer for an optimum window layer molar fraction found in the last section. Analysis was done separately for each output parameters in order to understand the effects more appropriately. The outcomes have been discussed, and the way of optimization of alloy composition at different layers was illustrated. Finally, a high efficiency design was proposed at the end of the chapter. Chapter 4 also analyses this new design against different input design parameters such as thickness of window layer, absorber layer, temperature. This chapter discusses the critical issues of fabrication, and brings necessary modifications in the designs of chapter 3 accordingly.

Overall, in this thesis, a modified solar cell structure was proposed, consisting of TCO/ZnO/$Cd_{1-x}Zn_xS$/$Cd_{1-x}Zn_xTe$/Cu_2Te/Ni, in which alloy composition was varied in the window layer in order to achieve a better windowing effect giving better J_{sc}. But it was accompanied by detrimental V_{oc} and FF, which were then improved by varying alloy composition in absorber layer that improved lattice matching. A small range of Zn x% around x = 0.2 appeared where the proposed two-fold treatment eventually yielded a better efficiency of 24.643%. The lattice mismatching of modified $Cd_{0.8}Zn_{0.2}S$/$Cd_{0.8}Zn_{0.2}Te$ was found to be 10.16%, which resembles the original CdS/CdTe lattice mismatch but yields better J_{sc} and V_{oc} that ultimately results in a high efficiency solar cell. The cell also showed very good temperature stability, giving an efficiency gradient of 0.05%/C^0. Further investigation was done to achieve optimization in thickness of window and absorber layer.

5.2 Major Contributions of the Work

The most important contribution of this research work is the introduction of a $Cd_{1-x}Zn_xS/Cd_{1-x}Zn_xTe$ heterojunction as the working p-n junction of a solar cell, replacing traditional CdS/CdTe solar cell. $Cd_{1-x}Zn_xTe$ is a less investigated material as the constituent of a solar cell, and it has only been tried in homojunction solar cells very recently [26]. The introduction of these two new ternary alloys present us with an opportunity to address the two fundamental drawbacks which traditional CdS/CdTe solar cell faces. The new window layer gives a better bandgap achieved through molar variation in ternary alloys. The new absorber layer employs the same molar alloy variation technique to improve the lattice mismatch with the modified window layer.

Another contribution of the work is the investigation into the output characteristics of the modified solar cell of $Cd_{0.8}Zn_{0.2}Te$ (lattice matched to $Cd_{0.8}Zn_{0.2}S$) for different input design scenarios such as varying thickness of window and absorber layer and varying temperature. The works done in chapter 3 and 4 provide useful insights into the optimization of design parameters and material properties for maximizing the efficiency level in II-VI solar cells.

5.3 Future Work

It is already mentioned that the window layer and absorber layer has significant lattice mismatch between them. This drawback was slightly improved, but can be improved further by choosing a buffer layer between window and absorber typically from II-VI compounds, which have lattice constant somewhere between that of the window and the absorber by means of advanced and improved fabrication processes [47-50]. We have options such as ZnSe or ZnTe that may replace the $Al_{0.9}Ga_{0.1}As$ buffer in III-V heterojunction solar cell for higher efficiency in near future. Similar ideas may apply to CdTe solar cell too.

Another development that can be done in our solar cell is to develop better BSF layer from the final design of section 3.3. Since the substrate is heavily ($\approx 10^{18}$ cm^{-3}) doped, it can work as a BSF layer in absence of the Cu_2Te layer (the reader is requested to refer to section 2.1.1 for the functional principle of the BSF layer) [51]. This will not change the results of section 3.3 significantly. As the substrate is very heavily doped with respect to the absorber, it can

effectively function as a BSF layer. So, we can have a thin film solar cell whose thickness can be further reduced (excluding substrate thickness), and yet yield similar efficiency.

Further research on TCO is going on, and improvement in this layer can significantly improve the overall efficiency and stability of thin film solar cells [52]. Research and development of p type TCO promises breakthrough advances in solar cell industry. The solar cell introduced in this work does not have an anti-reflective (AR) coating to reduce photon loss due to reflection, or a Bragg reflector that would increase the quantum efficiency of the cell. Including such layers in the solar cell would give higher efficiency [53].

Bibliography

1. Peter Gevorkian, *Sustainable energy systems engineering: the complete green building design resource*, p. 498, McGraw-Hill Professional, New York, USA, 2007, ISBN: 978-0071473590.

2. Marius Grundmann, *The Physics of Semiconductors: An Introduction Including Nanophysics and Applications*, 2nd ed., p. 3, Springer-Verlag, Berlin, Germany, 2010, ISBN: 978-3642138843.

3. K. A. Tsokos, *Physics for the IB Diploma*, 5th ed., Cambridge University Press, Cambridge, UK, 2008, ISBN: 978-0521708203.

4. Urjart. (2008) Solar Cell: Basic Principle of Operation. [Online]. Available: http://urjart.wordpress.com/2008/10/05/solar-cell-%E2%80%93-basic-principle-of-operation/

5. M. A. Green, "Solar cell fill factors: General graph and empirical expressions," *Solid-State Electronics*, vol. 24, no. 8, pp. 788-789, 1981.

6. Zh. I. Alferov, "Heterostructures and their applications in optoelectronics", *Akademiia Nauk SSSR*, vol. 7, pp. 28-40, 1976.

7. Stephen J. Fonash, *Solar Cell Device Physics*, 2nd Ed., Academic Press, Elsevier, Massachusetts, USA, 2010, ISBN: 978-0123747747.

8. U. S. Department of Energy. (2011) Energy Basics. [Online]. Available:http://www.eere.energy.gov/basics/renewable_energy/pv_cell_structures.html

9. Peter Wurfel, *Physics of Solar Cells: From Principles to New Concepts*, Wiley-VCH Verlag GmbH & Co. KGaA, Weinheim, Germany, 2005, ISBN: 3-527-40428-7

10. L. J. A. Koster, E. C. P. Smits, V. D. Mihailetchi, and P. W. M. Blom, "Device model for the operation of polymer/fullerene bulk heterojunction solar cells", *Physical Review B*, vol. 72, pp. 085205-1 - 085205-9, 2005, DOI: 10.1103/PhysRevB.72.085205

11. T. Tiedje, E. Yablonovitch, G. D. Cody, and B. G. Brooks, "Limiting efficiency of Silicon solar cells", *IEEE Transactions on Electron Devices*, vol. ED-31, pp. 711-716, 1984.

12. L.W. James,"III-V Compound heterojunction solar cells", in *Proceedings of IEEE International Electron Devices Meeting*, vol. 21, pp. 87-90, Washington, USA, 1975.

13. Alvin D. Compaan, Amorphous and Nanocrystalline Silicon Science and Technology, 2004, edited by Gautam Ganguly, Michio Kondo, Eric A. Schiff, Reinhard Carius, and Rana Biswas (Mater. Res. Soc. Symp. Proc. 808, Warrendale, PA, A7.6, 2004

14. Xuanzhi Wu,"High-efficiency polycrystalline CdTe thin-film solar cells", Solar Energy 77, pp.803, 2004.

15. M. S. Hossain, N. Amin, M. A. Matin, M.M. Aliyu, T. Razykov, K. Sopian, "A Numerical Study on The High Efficiency Ultra Thin $Zn_xCd_{1-x}S$/CdTe Solar Cell ", Chalcogenide Letters, vol.8, pp. 263-272, 2011.

16. Nowshad Amin, Kamaruzzaman Sopian, Makoto Konagai, "Numerical modeling of CdS/CdTe and CdS/CdTe/ZnTe solar cells as a function of CdTe thickness",Solar Energy Materials and Solar Cells (SOLMAT) 91,pp. 1202 , 2007.

17. D. L. Batzner, A. Romeo, H. Zogg, R. Wendt, A. N. Tiwari," Development of Efficient and Stable Back Contact CdTe/CdS Solar cell", Thin Solid Films 387, pp.151 , 2001.

18. X. Wu, J.C. Keane, R.G. Dhere, C. DeHart, D.S. Albin, A. Duda, T.A. Gessert, S. Asher, D.H. Levi, P. Sheldon, "16.5%-efficient CdS/CdTe polycrystalline thin-film solar cell", Proc. of 17th European Photovolt. Sol. Energy Conf, Munich, Germany, 2001.

19. Nowshad Amin, Akira Yamada and Makoto Konagai, "Effect of ZnTe and CdZnTe Alloys at the Back Contact of 1-μm-Thick CdTe Thin Film Solar Cells", Japanese Journal of Applied Physics 41(5A), Part 1, 2002.

20. I.O. Oladeji, L. Chow, C.S. Ferekides, V. Viswanathan, Z. Zhao," Metal/CdTe/CdS/$Cd_{1-x}Zn_xS$/TCO/glass: A new CdTe thin film solar cell structure", SOLMAT. 61, pp.203, 2000.

21. F.A. Abouel fotouh, R.Al Awadi, M.M. Abd-Elnaby," Growth optimization of $Zn_xCd_{1-x}S$ thin films by radio frequency magnetron co-sputtering for solar cell applications", Thin Solid Films 96, pp.169 , 1982.

22. S Chandrasekhar, S.Martinuzzi, F.Z.Nataren,"Improved Efficiency of CdZnS Thin Film Solar Cells", Canadian Journal of Physics 63, pp.716 , 1985.

23. P.R.Ram, R.Thangaraj, O.P. Agnihotri," Thin film CdZnS/$CuInSe_2$ solar cells by spray pyrolysis", Bulletin of Materials Science 8, pp.279 , 1986.

24. K.T.R. Reddy, P.J. Reddy, "Studies of $Zn_xCd_{1-x}S$ films and $Zn_xCd_{1-x}S$/$CuGaSe_2$heterojunction solar cells", Journal of Physics D: Applied Physics 25, pp.1345 , 1992.

25. R.N. Bhattacharya, M.A. Contreras, B. Egaas, R.N. Noufi, A. Kanevce, J.R. Sites, "Development of efficient and stable back contacts on CdTe/CdS solar cells, Thin Solid Films", Applied Physics Letters 89, 253503/1 , 2006.

26. O.M. Hussain, P.S. Reddy, B.S. Naidu, S. Uthanna, P.J. Reddy," Characterization of thin film ZnCdS/CdTe Solar cells", Sem. Sc. and Tech. 6, pp.690 , 1991.

27. I.O. Oladeji, L. Chow," Synthesis and Processing of CdS/ZnS Multilayer Films for Solar Cell Application", Thin Solid Films 474, pp.77, 2005.

28. L.C. Burton, T.L. Hench, "$Zn_xCd_{1-x}S$ films for use in heterojunction solar cells,", Appl. Phys. Lett. 29 (a), pp.612 , 1976.

29. T.L. Chu, S.S. Chu, J. Britt, C. Ferrikide and O.Q. Wu," Cadmium Zinc Sulfide Films and Heterojunctions", J. Appl. Phys. 70 (5), pp.2688, 1991.

30. S.Y. Yin, A.L. Fahrenbruch and R.H. Bube, "Chemical Solution Deposition of Inorganic Films",J. Appl. Phys. 49 (3), pp.1294 , 1978.

31. M.P. Valkonen, T. Kanniainien, S. Lindroos, M. Leskela and E. Rauhala,"Growth of ZnS, CdS and multilayer ZnS/CdS thin film by SILAR technique", Appl. Surf. Sci. 115, pp.386 1997.

32. M. Gunasekaran, M. Ichimura," Deposition of $Cd_{1-x}Zn_xS$ ($0 \leq x \leq 1$) Alloys by Photochemical Depositions", Japanese Journal of Applied Physics 44, pp.7345, 2005.

33. J. Zhou, X. Wu, G. Teeter, B. To, Y. Yan, R.G. Dhere, T. Gessert, "CBD $Cd_{1-x}Zn_xS$ thin films and there application in CdTe solar cell", Phy. St. Sol. 241(3), pp.775 , 2004.

34. M. Burgelman, J. Verschraegen, S. Degrave, P. Nollet, Prog." Modeling thin-film PV devices", Photovolt. Res. Appl., vol.12, pp.143, 2004.

35. S.J. Fonash et al., www.cneu.psu.edu/amps, accessed 2008.

36. M. Gloeckler, A. L. Fahrenbruch, and J. R. Sites, "Numerical Modeling of CIGS and CdTe Solar Cell: setting the baselines", Proceedings of the 3rd World Conf. on Photovoltaic Energy Conversion, May 11-18, , Osaka, Japan,pp.491-494, 2003.

37. Mohammadnor Imamzai, mohammadreza Aghaei, Nowshad Amin," Numerical modeling and analysis of CdS/$Cd_{1-x}Zn_xTe$ solar cells as a function of CdZnTe doping, lifetime and thickness", 4th International Conference on Photonics (ICP), IEEE, 2013.

38. T. Tiedje, E. Yablonovitch, G. D. Cody, and B. G. Brooks, "Limiting efficiency of Silicon solar cells", *IEEE Transactions on Electron Devices,* vol. ED-31, pp. 711-716, 1984.

39. B. G. Streetman, and S. K. Banerjee, *Solid State Electronic Devices,* 6th Ed., Prentice-Hall Inc., New Jersey, USA, 2006, ISBN: 978-8120330207.

40. M. A. Green, K. Emery, Y. Hishikawa, W. Warta, and E. D. Dunlop, "Solar cell efficiency tables (version 39)",*Progress in Photovoltaics: Research and Applications,* vol. 20, pp. 12-20, 2012..

41. M. Meyer, and R.A. Metzger, "Flying high: The Commercial Satellite Industry Convert to Compound Semiconductor Solar Cells", Compound Semiconductor, vol. 2, no. 6, pp. 22-24, 1996.

42. A. Goetzberger, C. Heblinga, and H. Schockb, "Photovoltaic materials, history, status and outlook", *Materials Science and Engineering: R: Reports,* vol. 40, no. 1, pp. 1-46, 2003.

43. A. S. Brown, U. K. Mishra, J. A. Henige, and M. J. Delaney, Journal of Vacuum Science & Technology B, vol. 6, no. 2, pp. 678-681, 1988.

44. Harish Palaniappan. (2012) Solar Cells. [Online]. Available: http://solar_cells.tripod.com/notes_sel_1.html

45. M. S. Leite, R. L. Woo, W. D. Hong, D. C. Law, and H. A. Atwater, "Wide-band-gap InAlAs solar cell for an alternative multijunction approach", *Applied Physics Letters,* vol. 98, pp. 093502-1 - 093502-3, 2011, DOI: 10.1063/1.3531756

46. J.W. Matthews, and A.E. Blakeslee, "Defects in epitaxial multilayers: I. Misfit dislocations", *Journal of Crystal Growth,* vol. 27, pp. 118- 125, 1974.

47. H. J. Scheel, P. Capper, *Crystal Growth Technology: From Fundamentals and Simulation to Large-scale Production,* p. 307, Wiley-VCH Verlag GmbH & Co. KGaA, Weinheim, Germany, 2008, ISBN: 978-3527317622

48. E. Popova, J. Faure-Vincent, C. Tiusan, C. Bellouard, H. Fischer, M. Hehn, F. Montaigne, M. Alnot, S. Andrieu, and A. Schuhl, "Epitaxial MgO layer for low-resistance and coupling-free magnetic tunnel junctions", *Applied Physics Letters,* vol. 81, no. 6, pp. 1035-1037, 2002.

49. P. K. Nayak, G. G. Belmonte, A. Kahn, J. Bisquert, and D. Cahen, "Photovoltaic efficiency limits and material disorder", *Energy and Environmental Science,* 2012, vol. 5, pp. 6022-6039, DOI: 10.1039/c2ee03178g

50. K. Van Nieuwenhuysen, F. Duerinckx, I. Kuzma, D. van Gestel, G. Beaucarne, J. Poortmans, "Progress in epitaxial deposition on low-cost substrates for thin-film crystalline silicon solar cells at IMEC", *Journal of Crystal Growth,* vol. 287, pp. 438–441, 2006.

51. J. G. Fossum, "Physical operation of back-surface-field silicon solar cells," *IEEE Transactions on Electron Devices,* vol. 24, no. 4, pp. 322-325, Apr. 1977.

52. Physical Technical Institute. (2005) NSM Archive - Physical Properties of Semiconductors. [Online]. Available: http://www.ioffe.ru/SVA/NSM/Semiconductor.

53. Harish Palaniappan. (2012) Solar Cells. [Online]. Available: http://solar_cells.tripod.com/notes_sel_1.html